AD_____

Award Number: DAMD 17-99-1-9492

TITLE: Neurofibromatosis 2 Tumor Suppressor Protein, Merlin, in Cellular Signaling to Actin Cytoskeleton

PRINCIPAL INVESTIGATOR: Vijaya Ramesh, Ph.D.

CONTRACTING ORGANIZATION: Massachusetts General Hospital
Boston, Massachusetts 02114

REPORT DATE: October 2000

TYPE OF REPORT: Annual

PREPARED FOR: U.S. Army Medical Research and Materiel Command
Fort Detrick, Maryland 21702-5012

REPORT DOCUMENTATION PAGE

Form Approved
OMB No. 074-0188

1. AGENCY USE ONLY (Leave blank)	2. REPORT DATE	3. REPORT TYPE AND DATES COVERED
	October 2000	Annual (1 Oct 99 – 30 Sep 00)

4. TITLE AND SUBTITLE
Neurofibromatosis 2 Tumor Suppressor Protein, Merlin, in Cellular Signaling to Actin Cytoskeleton

5. FUNDING NUMBERS
DAMD 17-99-1-9492

6. AUTHOR(S)
Vijaya Ramesh, Ph.D

7. PERFORMING ORGANIZATION NAME(S) AND ADDRESS(ES)
Massachusetts General Hospital
Boston, Massachusetts 02114

E-Mail:
ramesh@helix.mgh.harvard.edu

8. PERFORMING ORGANIZATION REPORT NUMBER

9. SPONSORING / MONITORING AGENCY NAME(S) AND ADDRESS(ES)
U.S. Army Medical Research and Materiel Command
Fort Detrick, Maryland 21702-5012

10. SPONSORING / MONITORING AGENCY REPORT NUMBER

11. SUPPLEMENTARY NOTES
This report contains colored photos

12a. DISTRIBUTION / AVAILABILITY STATEMENT
Approved for Public Release; Distribution Unlimited

12b. DISTRIBUTION CODE

13. ABSTRACT *(Maximum 200 Words)* The gene encoding the NF2 tumor suppressor showed a strong similarity to a family of cytoskeleton-associated proteins and was named merlin (for moesin-ezrin-radixin-like protein). The criticalquestion as to how the NF2 gene product, merlin, acts as a tumor suppressor largely remains unanswered because of the limited knowledge of the physiological function of merlin. Our studies reveal that merlin can bind to actin directly and isoform 2 of merlin which does not show self association bind actin more efficiently than isoform 1. We have also observed that merlin/ERM binding partner NHE-RF interacts with the PDGF receptor. Actin reorganization is an integral part of signal transduction pathways, and many of the signaling molecules interact with the actin cytoskeleton. In particular, the Rho family member Rac when activated by PDGF induces membrane ruffling. Our observaction that the translocation of endogenous merlin to membrane ruffles is stimulated by serum or PDGF, and the interaction of NHE-RF with the PDGF receptor strongly suggests a role for merlin in Rac mediated cellular signaling to actin cytoskeleton which will be the focus of our study in the next two year period.

14. SUBJECT TERMS	15. NUMBER OF PAGES
NF2, tumor suppressor, merlin, ERM proteins, PDGF, membrane ruffles	96
	16. PRICE CODE

17. SECURITY CLASSIFICATION OF REPORT	18. SECURITY CLASSIFICATION OF THIS PAGE	19. SECURITY CLASSIFICATION OF ABSTRACT	20. LIMITATION OF ABSTRACT
Unclassified	Unclassified	Unclassified	Unlimited

NSN 7540-01-280-5500

Standard Form 298 (Rev. 2-89)
Prescribed by ANSI Std. Z39-18
298-102

Table of Contents

Cover..... 1

SF 298..... 2

Table of Contents..... 3

Introduction..... 4

Body..... 4-6

Key Research Accomplishments..... 6

Reportable Outcomes..... 6

Conclusions..... 7

References..... 7

Appendices..... 4 papers enclosed

4. INTRODUCTION

Neurofibromatosis 2 (NF2) is a severe autosomal dominant disorder characterized by predisposition to a number of different tumors of the central nervous system, particularly vestibular and spinal schwannomas, and meningiomas. An important feature of NF2 is the bilateral occurrence of vestibular schwannomas. Similar tumors occur with higher frequency as sporadic unilateral lesions in the general population. The gene encoding the *NF2* tumor suppressor on chromosome 22q was isolated by positional cloning. The predicted protein product of this gene showed a strong similarity to a family of cytoskeleton-associated proteins and was named merlin (for **m**oesin-**e**zrin-**r**adixin-**l**ike prote**in**). We have established that the NF2 gene is inactivated in vestibular schwannomas and meningiomas. The critical question as to how the NF2 gene product, merlin, acts as a tumor suppressor largely remains unanswered because of the limited knowledge of the physiological function of merlin. The purpose of our research is to define the role of merlin in cellular signaling to actin cytoskeleton mediated primarily by the Rho family member Rac. Toward this goal we have completely characterized the interaction of merlin with actin and noted the differences that exist between the two isoforms of merln. Efforts are underway to place merlin in PDGF induced signaling to the actin cytoskeleton.

5. BODY

1. Characterization of merlin binding to G-and F-actin

As described in the statement of work, this work is now completed and a manuscript has been submitted for publication. The results are described briefly here and copies of the submitted manuscript are appended.

Merlin's homology to ERMs suggests it may possess similar functions, acting as a link between cytoskeletal components and the cell membrane. The N-terminus of merlin has strong sequence identity to the N-terminal actin-binding region of ezrin. We therefore undertook a detailed study to characterize the merlin-actin interaction. We have observed that merlin isoform 1 and 2 differentially bind actin filaments, suggesting that the intramolecular interactions in isoform 1 may hinder its ability to bind actin. Merlin isoform 2 binds F-actin with an apparent binding constant of 3.6 μM and a stoichiometry of 1 mole merlin per 11.5 moles of actin in filaments at saturation and does not bind G-actin. Merlin isoform 2, and the N-terminal domain, slow actin filament disassembly further demonstrating that merlin binds periodically along F-actin. Merlin distributes into the cytoskeletal fraction of meningioma cells and immunogold electron microscopy shows it to be bound on cytoskeletal actin filaments, particularly near their ends where they intersect with one another at the cortical cytoskeleton. Comparison of these findings to those reported for ERM proteins reveal a distinct role for merlin in actin filament dynamics (James et al., manuscript submitted, see appendix). In the coming year as originally

proposed we will focus on defining the role of merlin in signal transduction pathways involving small GTPases particularly Rac.

2. NHE-RF interaction with the PDGF receptor

We have identified human NHE-RF as an interactor for merlin and its relatives, moesin and radixin [1]. NHE-RF was independently isolated as an interactor for ERM proteins which was named EBP50 (for ERM binding protein 50 kD) [2]. Our recent studies demonstrate that merlin isoform 2 exhibits stronger interaction for NHE-RF when compared to isoform 1 consistent with our earlier observation that merlin isoform 2 does not exist in a dormant form, a feature that is different from merlin isoform 1 and other ERM proteins [3]. NHE-RF possesses two PDZ domains, known to mediate protein-protein interactions, particularly at the plasma membrane forming a multiprotein complex involved in cellular signaling. Thus NHE-RF appears to function as a key adaptor protein linking a variety of ion channles and receptors from the plasma membrane to the actin cytoskeleton. Based on the consensus motif described for the PDZ1 domain of NHE-RF, we predicted that NHE-RF would interact with the PDGF receptors PDGFR-A and PDGFR-B. Our ongoing studies clearly suggest that the PDGFR-B is capable of interacting with NHE-RF (unpublished results). We are currently analyzing the actin reorganization induced by PDGF in PDGFR null cells derived from knock out mice, in comparison with cells where either wild type or mutant receptor not capable of interacting with NHE-RF are expressed. We anticipate that our will establish the involvement of merlin-NHE-RF interaction in the PDGF induced actin cytoskeleton reorganization.

In addition, in collaboration with other investigators we have established that NHE-RF is capable of interacting with the B1 subunit of H^+ATPase (Breton et al., J. Biol. Chem. 275: 18219, 2000) as well as mammalian Trp4 and Phospholipase C isozymes (Tang et al., J. Biol. Chem. 2000, in press). Copies of these papers are appended.

3. NHE-RF is upregulated in estrogen receptor positive breast carcinomas

During our analysis of NHE-RF expression in a variety of cell lines derived from human tumors including breast tumors, ovarian tumors, colon carcinomas and meningiomas we noticed an upregulation of NHE-RF in a subset of breast cancer cell lines. Interestingly these cell lines were derived from estrogen positive breast tumors. NHE-RF expression is upregulated in response to estrogen in estrogen receptor (ER)-positive breast carcinoma cell lines, suggesting that it may be involved in estrogen signaling. To further understand NHE-RF function and its possible role in estrogen signaling, we analyzed NHE-RF expression in normal human tissues, including cycling endometrium, and in breast carcinomas, tissues in which estrogen plays an important role in regulating cell growth and proliferation. NHE-RF is expressed in many epithelia, especially in cells specialized in ion transport or absorption, and is often localized to apical (luminal) membranes. NHE-RF expression varies markedly in proliferative versus secretory endometrium, with high expression in proliferative (estrogen-stimulated) endometrium.

Furthermore, ER status and NHE-RF expression correlate closely in breast carcinoma specimens. These findings support a role for NHE-RF in estrogen signaling. A manuscript detailing this work is accepted for publication and appended (Stemmer- Rachamimov et al., Amer. J. Pathol. in press).

To further understand the estrogen mediated regulation of NHE-RF, we are continuing our efforts to define the critical elements in the NHE-RF gene that are responsible for this upregulation. Toward this, we have isolated genomic clones encoding NHE-RF gene and further characterization of the promoter region is underway.

6. KEY RESEARCH ACCOMPLISHMENTS

* Qunatitative characterization of merlin binding actin and functional significance (manuscript submitted)

* Merlin partner NHE-RF binding to PDGF receptor (unpublished, in progress)

* NHE-RF binding to H+ATPase, mammalian Trp4 and Phospholipase C (J.Biol. Chem. 275, 2000; J. Biol. Chem. in press)

* Upregulation of NHE-RF expression in estrogen receptor positive breast carcinomas (Amer J. Pathol. in press)

7. REPORTABLE OUTCOME

Manuscripts:

Breton S, Wiederhold T, Marshansky V, Nsumu N, Ramesh V, Brown D. (2000) The B1 subunit of the H^+ATPase is a PDZ-domain binding protein: colocalization with NHE-RF in renal B-intercalated cells. J. Biol. Chem. 275, 18219-18224.

Tang Y, Tang J, Chen Z, Trost C, Flockerzi V, Li M, Ramesh V, and Zhu M. (2000) Association of mammalian Trp4 and phospholipase C isozyme with a PDZ domain-containing protein, NHE-RF. J. Biol. Chem. (in press).

Stemmer-Rachamimov A, Wiederhold T, Nielsen P, James M, Pinney-Michalowski D, Roy JE, Cohen WA, Ramesh V and Louis D. (2000) NHE-RF, a merlin interacting protein is primarily

expressed in luminal epithelia, proliferative endometrium and estrogen receptor-positive breast carcinomas. Amer. J. Pathol. (in press).

James M, Manchanda N, Gonzalez-Agosti C, Hartwig J, and Ramesh V. (2000) Merlin selectively binds F- but not G-actin, and stabilizes the filaments through a lateral association. Submitted.

Presentation:

Part of the work was presented at the NNFF international consortium for the molecular biology of NF1 and NF2 held at Aspen, Colorado in June 2000.

8. CONCLUSION

We strongly believe that merlin is a player in the Rho/Rac mediated signaling to actin cytoskeleton. We have completed the studies that we proposed to finish in the first year (as mentioned in the statement of work) and well on our way with other proposed experiments that include NHE-RF interaction with PDGFR and to understand the involvement of merlin in cellular signaling cascade to the cytoskeletal network. We do not anticipate any major changes in the original proposed work. However, since NHE-RF is clearly regulated by estrogen and upregulated in estrogen receptor (ER) positive breast cancer, we will identify the elements that are necessary for this upregulation in ER positive breast tumors. We expect that the results generated will provide new directions to follow to further define the role of NHE-RF in estrogen signaling.

9. REFERENCES

1. Murthy A, Gonzalez-Agosti C, Cordero E, Pinney D, Candia C, Solomon F, Gusella J, Ramesh V (1998) NHE-RF, a regulatory co-factor for Na+-H+ exchange is a common interactor for merlin and ERM proteins. J. Biol. Chem. 273:1273-1276

2. Reczek D, Berryman M, Bretcher A (1997) Identification of EBP50: A PDZ-containing phosphoprotein that associates with members of the ezrin-radixin-moesin family. J. Cell Biol. 139:169-179

3. Gonzalez-Agosti C, Wiederhold T, Herndon ME, Gusella J, Ramesh V (1999) Interdomain interaction of merlin isoforms and its influence on intermolecular binding to NHE-RF. J. Biol. Chem. 274:34438-34442

10. APPENDIX

4 Papers enclosed

APPENDIX

THE JOURNAL OF BIOLOGICAL CHEMISTRY
Vol. 275, No. 24, Issue of June 16, pp. 18219–18224, 2000
Printed in U.S.A.

The B1 Subunit of the H$^+$ATPase Is a PDZ Domain-binding Protein

COLOCALIZATION WITH NHE-RF IN RENAL B-INTERCALATED CELLS*

Received for publication, December 13, 1999, and in revised form, March 2, 2000
Published, JBC Papers in Press, March 30, 2000, DOI 10.1074/jbc.M909857199

Sylvie Breton‡§¶, Thorsten Wiederhold‖, Vladimir Marshansky‡, Ndona N. Nsumu‡, Vijaya Ramesh§‖, and Dennis Brown‡ ‡‡**

From the ‡Renal Unit and Program in Membrane Biology and the ‖Molecular Neurogenetics Unit, Massachusetts General Hospital East, Charlestown, Massachusetts 02129 and the Departments of ‡‡Pathology and §Medicine, Harvard Medical School, Boston, Massachusetts 02114

The 56-kDa B1 subunit of the vacuolar H$^+$ATPase has a C-terminal DTAL amino acid motif typical of PDZ-binding proteins that associate with the PDZ protein, NHE-RF (Na$^+$/H$^+$ exchanger regulatory factor). This B1 isoform is amplified in renal intercalated cells, which play a role in distal urinary acid-base transport. In contrast, proximal tubules express the B2 isoform that lacks the C-terminal PDZ-binding motif. Both the B1 56-kDa subunit and the 31-kDa (E) subunit of the H$^+$ATPase are pulled down by glutathione S-transferase NHE-RF bound to GSH-Sepharose beads. These subunits associate *in vivo* as part of the cytoplasmic V1 portion of the H$^+$ATPase, and the E subunit was co-immunoprecipitated from rat kidney cytosol with NHE-RF antibodies. The interaction of H$^+$ATPase subunits with NHE-RF was inhibited by a peptide derived from the C terminus of the B1 but not the B2 isoform. NHE-RF colocalized with H$^+$ATPase in either the apical or the basolateral region of B-type intercalated cells, whereas NHE-RF staining was undetectable in A-intercalated cells. In proximal tubules, NHE-RF was located in the apical brush border. In contrast, H$^+$ATPase was concentrated in a distinct membrane domain at the base of the brush border, from which NHE-RF was absent, consistent with the expression of the truncated B2 subunit isoform in this tubule segment. The colocalization of NHE-RF and H$^+$ATPase in B- but not A-intercalated cells suggests a role in generating, maintaining, or modulating the variable H$^+$ATPase polarity that characterizes the B-cell phenotype.

Membrane transport proteins are directed toward and inserted into specific cell surface domains by an elaborate series of sorting mechanisms (1). A relatively recent development in understanding how some of these proteins are concentrated into functionally differentiated regions of the plasma membrane has been the discovery of the so-called PDZ domain family of proteins and associated PDZ-binding proteins. Named after the initial three members of the family (PSD-95, *Drosophila* discs large protein, and ZO-1), PDZ proteins contain 80–100-amino acid stretches that allow them to interact with other proteins that have a four amino acid PDZ-binding cassette, usually at the extreme C terminus of the cytoplasmic domain (2). One such PDZ-binding cassette is the amino acid sequence D(S/T)XL. Thus, putative PDZ-binding proteins can be identified by screening their amino acid sequence for these concensus cassettes. Among the many proteins identified so far are the cystic fibrosis transmembrane conductance regulator (3), the β_2-adrenergic receptor (4), neuronal nitric-oxide synthase (5), GLUT1 (6), and some potassium channels (7–9). One PDZ protein to which the cystic fibrosis transmembrane conductance regulator (10), the β_2-adrenergic receptor, and P2Y1 receptor (4) bind is the Na$^+$/H$^+$ exchanger regulatory factor, NHE-RF, originally identified in rabbit kidney as a soluble factor that participates in the regulation of the NHE-3 Na$^+$/H$^+$ exchanger at the apical pole of proximal tubule epithelial cells (11, 12). NHE-RF also binds to the ERM family of actin-binding proteins via its C terminus outside the PDZ-binding motif (13, 14), thus potentially linking many ion channel and receptors to the actin cytoskeleton. Furthermore, NHE-RF has been reported to interact with the Na$^+$/HCO_3^- co-transporter, a basolateral protein in proximal tubules (15).

The B1 (56-kDa) subunit of the vacuolar proton-pumping ATPase (H$^+$ATPase) has a C-terminal DTAL motif, which suggests that it is a candidate PDZ-binding protein. This subunit of the H$^+$ATPase is expressed in several tissues, but it is strongly amplified in specialized proton-translocating intercalated cells in the kidney (16), as well as similar cells in the epididymis (17). In contrast, a highly homologous 56-kDa isoform, the B2 isoform, is expressed in the kidney proximal tubule, but it has a C-terminal truncation and lacks the terminal PDZ-binding cassette (16). Most if not all of the PDZ-binding proteins so-far reported are transmembrane proteins, but the B1 H$^+$ATPase subunit is part of the V1 portion of the holo-enzyme and has no membrane spanning domain. It is tethered to the membrane by interaction with other subunits of the enzyme, some of which span the lipid bilayer (18). Furthermore, multi-subunit complexes consisting of the cytoplasmic portion of the H$^+$ATPase can exist as free, cytosolic entities (18).

In kidney cortex, intercalated cells show a complex regulation of H$^+$ATPase expression at the cell surface (19), and subpopulations of these cells with apical, basolateral, diffuse, or even bipolar H$^+$ATPase localization can be detected by immunocytochemistry (20). A-cells always have H$^+$ATPase at their apical pole and the Cl^-/HCO_3^- exchanger AE1 at their basolateral pole (21). These cells secrete protons into the tubule lumen. B-cells have no detectable AE1 in either plasma mem-

* This work was supported by National Institutes of Health Grants DK38452 (to S. B.), DK42956 (to D. B.), and NS24279 (to V. R.) and by a U.S. Army grant (to V. R.). The costs of publication of this article were defrayed in part by the payment of page charges. This article must therefore be hereby marked "*advertisement*" in accordance with 18 U.S.C. Section 1734 solely to indicate this fact.

¶ Supported by a Massachusetts General Hospital Claflin Distinguished Fellowship. To whom correspondence should be addressed: Renal Unit and Program in Membrane Biology, Massachusetts General Hospital East, 149 13th St., Charlestown, MA 02129. Tel.: 617-726-5785; Fax: 617-726-5669; E-mail: sbreton@receptor.mgh.harvard.edu.

** Supported by a Gottlieb Daimler and Karl Benzs Predoctoral Fellowship.

brane domain, but the H⁺ATPase can be apical, basolateral, or bipolar in these AE1-negative cells. Cells with basolateral H⁺ATPase are bicarbonate-secreting cells. Although systemic acidosis results in more intercalated cells having apical H⁺ATPase, and alkalosis shifts more cells to a basolateral pattern of localization (22, 23), the cell biological mechanisms underlying these dramatic shifts in the polarized expression of a membrane protein remain unknown *in situ*. In this report, we show that the 56-kDa B1 subunit of the proton pump is a PDZ-binding protein that can associate with NHE-RF and that NHE-RF colocalizes with the H⁺ATPase in all B-intercalated cells, wherever the pump is located within any individual cell. We propose that the interaction of this subunit of the proton pump with NHE-RF could be responsible for the anchoring and/or targeting of membrane-associated H⁺ATPase molecules in this cell type. NHE-RF was barely detectable in A-type intercalated cells. In contrast, NHE-RF was abundant in the proximal tubule brush border, but its intracellular location was clearly distinct from that of the H⁺ATPase in these cells.

EXPERIMENTAL PROCEDURES

Animals—Male Harlan Sprague-Dawley rats were anesthetized with sodium pentobarbital (Nembutal, 0.1 ml of a 50 mg/ml solution/100 g of body weight), and kidneys were fixed by perfusion through the abdominal aorta with a fixative containing 4% paraformaldehyde, 10 mM sodium periodate, 70 mM lysine (PLP), and 5% sucrose as described previously (24, 25). After 5 min of perfusion, kidneys were removed, sliced, and fixed by immersion for a further 6 h before rinsing and storage in PBS[1] (10 mM sodium phosphate buffer containing 0.9% NaCl, pH 7.4). For preparation of 4-μm sections, tissues were cryoprotected in 30% sucrose before sectioning with a Reichert Frigocut microtome using disposable knives.

Immunostaining—Tissue sections picked up on Fisher Superfrost Plus slides (Fisher Scientific) were rinsed for 10 min in PBS and then treated with 1% SDS for 5 min. This step augments antigenicity of many proteins in frozen sections of PLP-fixed tissues, as described previously (26). After three more rinses (5 min each) in PBS to remove the SDS, sections were incubated for 20 min in PBS/1% bovine serum albumin to block nonspecific background staining. Primary anti-NHE-RF antibody (affinity purified rabbit polyclonal antibody IC270 raised against GST-NHE-RF fusion protein amino acids 270–358) was applied for 2 h at room temperature at a dilution of 1:4. This antibody has been characterized previously (27). After washing twice for 5 min in high salt PBS (PBS containing 2.7% NaCl) to reduce nonspecific staining and one further washing for 5 min in normal PBS, secondary anti-rabbit antibodies (diluted 1:800) coupled to CY3 (Jackson Immunologicals) were applied for 60 min. After further washing as above, sections were mounted in Vectashield anti-fading solution (Vector Labs., Burlinghame, CA), diluted 1:1 in 0.1 M Tris-HCl, pH 8.0.

Some sections were double-stained with anti-H⁺ATPase antibodies to identify the cells that were positive for NHE-RF in the collecting duct. After application of the anti-NHE-RF antibody followed by secondary antibody coupled to CY3, an affinity purified chicken polyclonal antibody against the 31-kDa E subunit of the H⁺ATPase (a marker of A- and B-intercalated cells, diluted 1:40) was applied for 2 h, followed by a donkey anti-chicken IgG coupled to FITC, diluted 1:200 (Jackson Immunologicals). Sections were mounted in Vectashield diluted 1:1 in 0.1 M Tris-HCl, pH 8.0.

Some sections were double stained using a rabbit anti-AE1 Cl^-/HCO_3^- exchanger antibody that has been previously characterized (28). Because this antibody is also raised in rabbit, an amplification procedure was used to allow staining of sections with two primary antibodies raised in the same species. Briefly, the first primary, anti-AE1, was applied at a dilution of 1:32,000, a concentration that is too low to be detected by conventional application of a fluorescent secondary antibody, as determined in preliminary experiments. The dilute AE1 antibody was detected using a tyramide amplification kit (NEN Life Science Products) with tyramide-CY3 as a fluorescent reagent, according to the manufacturer's instructions. The sections were then incubated conventionally with anti-NHE-RF and secondary goat anti-rabbit FITC as described above. No cross-reactivity between the two sets of reagents was detectable under these conditions. Sections were photographed in color on Kodak Ektachrome 400 Elite film exposed at 2500 ASA using a Nikon Eclipse 800 epifluorescence microscope equipped with specific CY3 and FITC filter combinations. Using the specific CY3 filter combination and analog photography, CY3 emission appears yellow (see Fig. 1, *A* and *C*). Some micrographs were prepared from digital images captured from the Nikon Eclipse 800 using a Hamamatsu Orca digital camera. Pseudocolored images were merged using IP Lab Spectrum software (Scanalytics Inc, Vianna). In these images, CY3 fluorescence appears *red*, and FITC is *green* (see Fig. 2). Control incubations were performed in which the primary NHE-RF antibody was incubated with the GST-NHE-RF fusion protein (at a final concentration of 0.2 mg/ml) for 1 h at room temperature prior to applying the antibody to the sections.

Preparation of Rat Kidney Inner Stripe Cytosol—Kidneys of anesthetized rats were perfused with cold PBS for 1–2 min to remove blood, and the inner stripe was separated under a dissecting microscope. Pieces of inner stripe (0.4 g) were homogenized in 2 ml of homogenization buffer (0.25 M sucrose, 1 mM EDTA, 10 mM Tris-HCl, pH 7.4, with Complete™, Roche Molecular Biochemicals, mixture of protease inhibitors) using a Wheaton glass potter fitted with a Teflon pestle (20 complete strokes). Rat kidney inner stripe cytosol was prepared by centrifugation of the homogenate for 1 h at 100,000 × *g* (41,000 rpm) using a Beckman, TL-100 Ultracentrifuge equipped with a TLA 55 rotor. Protein concentration of cytosol was measured with the Pierce BCA protein assay reagent using albumin as a standard.

Affinity Precipitation and Peptide Competition Assay—Pull-down experiments were performed essentially as described previously (27) with minor modifications. Briefly, rat kidney inner stripe cytosol (0.4 mg of total protein) was incubated overnight at 4 °C with 600 pmol of GST-NHERF or GST alone as a control immobilized on GSH-Sepharose 4B beads. For the peptide competition assay, peptides B1 (PQDTEADTAL) and B2 (EFYPRDSAKH) were dissolved in distilled water, and 300 μg of peptide were preincubated with the GST-NHE-RF beads for 1 h at 4 °C. Cytosol containing 300 μg of peptide was then added to the beads, and the mixture was incubated overnight at 4 °C. The beads were then washed extensively with phosphate-buffered saline containing Pefabloc and resuspended in Laemmli sample buffer for SDS-PAGE.

Immunoprecipitation Assay—Rat kidney cytosol was prepared as for the pull-down assay, except that cytosol from the entire cortex and outer medulla was used to ensure that adequate amounts of NHE-RF were present in the preparation. NHE-RF was immunoprecipitated from 500 μl (2.8 mg of total protein) of precleared (by preincubation with protein A-agarose beads alone) cytosol using 10 μl of anti-NHE-RF antiserum (IC270 serum or IC270 preimmune serum) and 50 μl of protein A-agarose beads (Roche Molecular Biochemicals). Immunoprecipitates were washed extensively with PBS and eluted by boiling in SDS sample buffer (as for the pull-down assay). The immunoprecipitates were run on SDS-PAGE and blotted using a monoclonal anti-E subunit antibody (E11) as described below.

SDS-PAGE and Western Blot Analysis—Electrophoresis was performed using 12% SDS-Tris-glycine-PAGE gels. Proteins were transferred to polyvinylidene difluoride membranes and analyzed by Western blotting. The following antibodies were used as detailed in the figure legends: affinity-purified chicken polyclonal anti-E H⁺ATPase subunit (1:1,000) and affinity-purified rabbit polyclonal anti-B1 H⁺ATPase subunit (1:1,000), raised against the bovine subunits, and a monoclonal anti-E subunit antibody (E11) kindly provided by Dr. Steven Gluck (University of Florida, Gainesville). Images were scanned and analyzed with NIH Image (version 1.62) software.

RESULTS

Localization of NHE-RF in the Kidney—NHE-RF was localized in the kidney on PLP-fixed cryostat sections that had been treated with SDS. As expected from the reported distribution of NHE-3 (29), by far the greatest amount of NHE-RF was found in proximal tubules. The entire brush border was strongly stained in all proximal tubule segments (Fig. 1, *A* and *C*). In addition, however, staining was seen in some cells of the cortical collecting ducts and connecting segments (Fig. 1, *A* and *C*). The extent and intracellular location of this staining was variable, with some cells showing distinct basolateral staining (Fig. 1*A*), others showing a more diffuse cytoplasmic staining (Fig. 1*C*), and yet others showing apical staining (Fig. 1*C*). These cells were identified as intercalated cells by double incubations

[1] The abbreviations used are: PBS, phosphate-buffered saline; GST, glutathione *S*-transferase; FITC, fluorescein isothiocyanate; PAGE, polyacrylamide gel electrophoresis.

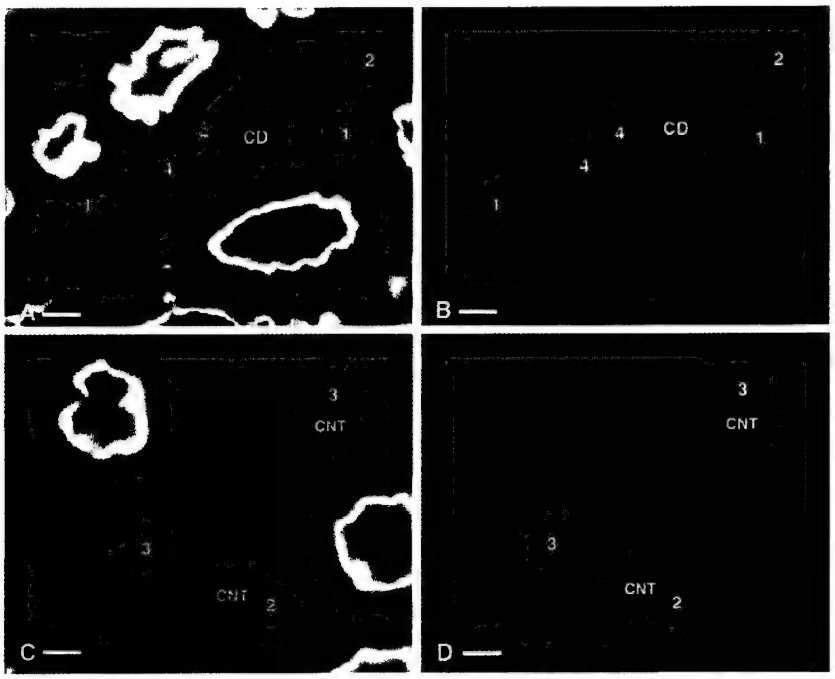

FIG. 1. Sections of rat kidney cortex double stained for NHE-RF (*A* and *C*) and the 31-kDa subunit of the H⁺ATPase (*B* and *D*). The brush border is strongly stained in all proximal tubules. Some cells of the collecting ducts (*CD*) and connecting segments (*CNT*) are also stained. Different patterns of NHE-RF staining are detected, and the staining overlaps with that of the H⁺ATPase in intercalated cells. Some cells have basolateral staining (*1*), some have diffuse cytoplasmic staining (*2*), some have apical staining (*3*), and others have little or no NHE-RF staining but show apical H⁺ATPase staining (*4*). In connecting segments (CNT), all cells have strong H⁺ATPase staining, as described previously (30), but only a few of these are clearly NHE-RF-positive. The staining in *A* and *C*, which represent single exposures of the NHE-RF staining, appears *yellow* because of the use of a highly specific filter combination used for the CY3 fluorophore. Cy3 emission is *yellow* when the correct filter combination is used. *Bar*, 15 μm.

using a chicken polyclonal antibody against the 31-kDa (E) subunit of the H⁺ATPase (Fig. 1, *B* and *D*). We have previously shown that the three major subunits of the cytoplasmic domain of this enzyme colocalize in intercalated cells (30). Thus, the E subunit is a reliable marker for the entire cytoplasmic domain of the H⁺ATPase, which also contains the 56 B kDa subunit. In these double-stained sections, the NHE-RF staining colocalized with the H⁺ATPase staining in intercalated cells, whereas connecting tubule cells that also contain the H⁺ATPase do not express detectable levels of NHE-RF (Fig. 1, *C* and *D*). However, in some intercalated cells, apical H⁺ATPase staining was seen with no detectable NHE-RF staining (Fig. 1*A*). Principal cells in some tubule segments showed a faint, finely granular staining in the cytoplasm that was much less intense than in the adjacent intercalated cells.

To distinguish between A- and B-intercalated cells, anti-AE1 antibodies, which label only A-cells (21), were used in conjunction with anti-NHE-RF antibodies. All cells with distinct apical, diffuse, or basolateral NHE-RF staining were negative for AE1 (Fig. 2). Furthermore, only A-intercalated cells are found in the inner stripe of the outer medulla, and these cells showed no detectable staining with the NHE-RF antibody (not shown). Thus, NHE-RF is most highly expressed in B-intercalated cells, and its variable intracellular localization pattern overlaps with that of the H⁺ATPase in each individual B-cell in the cortical collecting duct and connecting segment.

In proximal tubules, NHE-RF was present in the brush border (Fig. 3), as predicted from previous studies that showed abundant NHE-3 in this location (11, 29). However, the H⁺ATPase staining was, as we have previously described (30), the most concentrated in a tight subapical band at the base of the brush border. This subapical domain, showing intense

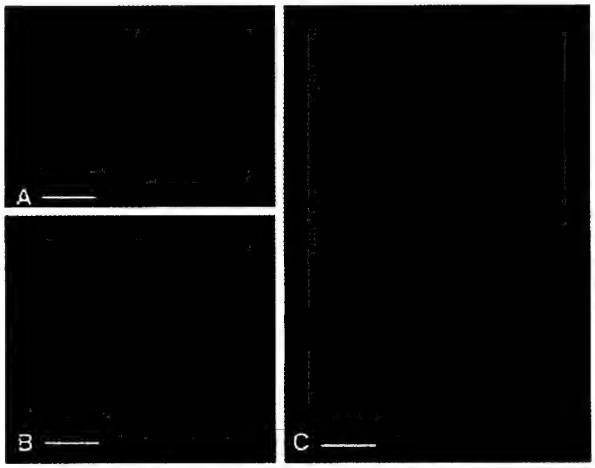

FIG. 2. Double staining of rat kidney cortex collecting ducts with antibodies against NHE-RF (***green***) and AE1 (***red***). The *red* AE1 staining is basolateral in all A-intercalated cells. These cells do not stain for NHE-RF. In *A*, two cells with apical NHE-RF staining are found alongside an A-intercalated cell with basolateral AE1 staining. In *B*, two cells with basolateral NHE-RF staining are found in the same tubule as A-intercalated cells with basolateral AE1. Other cells are negative for both antigens. *C* shows a collecting duct with a mixture of AE1 positive/NHE-RF negative A-intercalated cells and NHE-RF-positive/AE1-negative B-intercalated cells. A small amount of punctate NHE-RF staining is seen in cells that are probably principal cells. In these merged digital images, CY3 staining is pseudocolored *red* to allow it to be more readily distinguished from the adjacent *green* FITC staining. *Bar*, 10 μm.

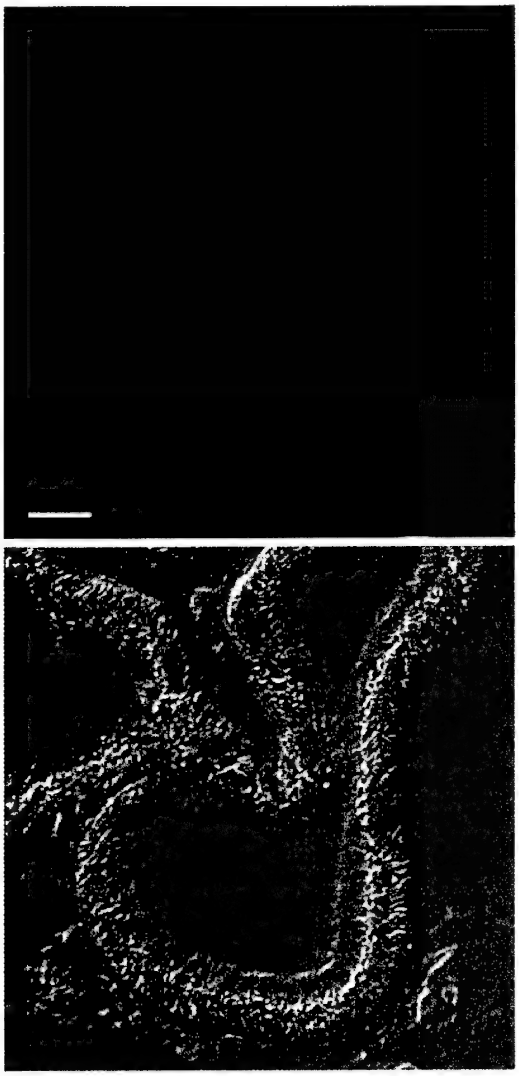

FIG. 3. Proximal tubule from rat kidney cortex showing the distribution of NHE-RF (*red*) on the brush border microvilli, and the H⁺ATPase (31-kDa subunit; *green*) on submicrovillar vesicles and invaginations. The two proteins are not co-localized in this S3 tubule segment. A differential interference contrast image is shown in the *lower panel* for orientation purposes. *Bar*, 10 μm.

H⁺ATPase staining in the S3 segment, did not contain detectable levels of NHE-RF (Fig. 3). This is consistent with the known expression of the C-terminally truncated B2 isoform of the 56-kDa subunit in these cells, which lacks the DTAL PDZ-binding motif (16). NHE-RF was not detected in the basolateral domain of proximal tubules.

To determine the specificity of labeling with anti-NHE-RF antibodies in kidney cortex, parallel incubations were performed with normal anti-NHE-RF antibody and with antibody that had been preincubated with 0.2 mg/ml of the GST-NHE-RF fusion protein that was used as an immunogen. The results show that the proximal tubule staining, as well as the apical, basolateral, and bipolar intercalated cell staining were completely abolished by preincubation with the immunizing fusion protein (Fig. 4).

Binding of Soluble H⁺ATPase Complexes to a GST-NHE-RF Affinity Matrix—Sepharose beads to which a GST-NHE-RF fusion protein was bound were used as an affinity matrix to

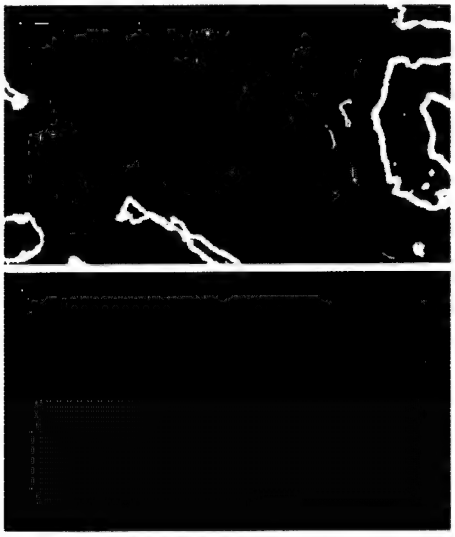

FIG. 4. Control for the specificity of NHE-RF staining in rat renal cortex. Under normal incubation conditions (*A*), NHE-RF stains the brush border of proximal tubules, as well as intercalated cells in variable patterns (apical, basolateral, and bipolar). This staining is completely inhibited by preincubation of the NHE-RF antibody with the immunizing GST-NHE-RF fusion protein (*B*). *Bar*, 10 μm.

extract potential binding proteins from renal medullary cytosol. A cytosolic preparation from the inner medulla was used for these experiments because (*a*) kidney cytosol contains large amounts of free cytosolic H⁺ATPase subunits (Fig. 5*A*, *Cytosol*), (*b*) this kidney region contains high levels of the B1-H⁺ATPase isoform, located in A-type intercalated cells, and (*c*) this region contains no proximal tubules, which express abundant endogenous NHE-RF that could potentially compete with protein binding to the affinity matrix. Under these conditions, Western blots of the affinity-purified material bound to the beads showed that both the B1 and the E subunits of the H⁺ATPase were present (Fig. 5*A*). Control experiments using the matrix with GST alone showed little or no H⁺ATPase subunit antigenicity associated with the beads in the absence of NHE-RF, indicating the specificity of the association. The binding of H⁺ATPase to the NHE-RF-GST affinity matrix was completely inhibited by incubation of the beads with an 11-amino acid C-terminal peptide derived from the B1 H⁺ATPase subunit, which contains the C-terminal motif DTAL (PQDTEADTAL). However, binding was not inhibited by preincubation with a peptide containing the 11 C-terminal amino acids of the B2 56-kDa subunit isoform (EFYPRDSAKH), which does not contain the PDZ-binding motif (Fig. 5*B*).

Co-immunoprecipitation of NHE-RF and the H⁺ATPase—to strengthen the evidence for an *in vivo* interaction between NHE-RF and the H⁺ATPase, evidence for co-immunoprecipitation of the two proteins from rat kidney cytosol was sought. As shown in Fig. 5*C*, the E subunit of the H⁺ATPase was co-immunoprecipitated from kidney cytosol by the anti-NHE-RF antibody but not by preimmune serum.

DISCUSSION

The present data show that the 56-kDa B1 subunit isoform of the H⁺ATPase is a PDZ-binding protein that allows association of the cytosolic (V1) portion of the H⁺ATPase with NHE-RF, a PDZ protein that is expressed in the kidney. Immunolocalization indicates that in the collecting duct and connecting segment, this association occurs in a specialized subtype of intercalated cell, the B-cell, which has a highly variable pattern of intracellular localization of the H⁺ATPase (19–21, 23). Other

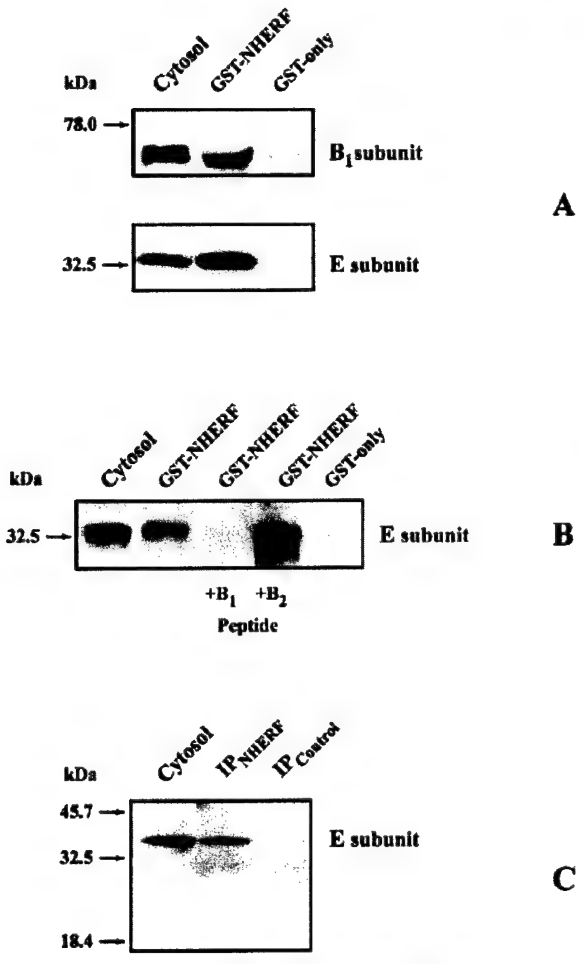

FIG. 5. Results of the GST-NHE-RF pull down assay and co-immunoprecipitation. *A* shows that both the B1 and the E H⁺ATPase subunits are pulled down by GST-NHERF beads, but not by beads coupled to GST alone. *B* shows that the ability of the GST-NHERF beads to pull down the H⁺ATPase (in this case the E subunit) is completely inhibited by a peptide derived from the B1 H⁺ATPase subunit (which contains the DTAL motif) but is not competed away by the B2 subunit peptide. *C* shows that the E subunit of the H⁺ATPase is co-immunoprecipitated by anti-NHE-RF antibodies but not by preimmune serum. In all of these blots, the E subunit runs slightly higher than the predicted 31-kDa molecular mass for this subunit. *IP*, immunoprecipitate.

collecting duct cell types, including principal cells and A-intercalated cells, showed a very low level of staining. The greatest amount of NHE-RF staining was observed, as expected in proximal tubules, but some thin limbs of Henle in the medulla were also strongly stained (not shown).

Especially intriguing is the failure to detect NHE-RF in A-type intercalated cells, which also contain high levels of the B1-H⁺ATPase subunit but which always have an apical staining for this protein, either on the plasma membrane or on numerous subapical vesicles. Thus, NHE-RF expression is amplified in the AE1-negative B-cell population, in which the pattern of H⁺ATPase localization is widely variable. This result suggests that the B-cell represents a distinct cell type with respect to NHE-RF expression and that NHE-RF could be involved in generating and/or maintaining apical and basolateral H⁺ATPase polarity in B-cells. Because A-cells, which insert H⁺ATPase uniquely into the apical domain, contain little or no detectable NHE-RF, we conclude that NHE-RF is in some way involved in the ability of B-cells to display plasticity of membrane H⁺ATPase insertion. This could occur via the association of NHE-RF with merlin and/or ezrin, members of the ERM (ezrin, radixin, moesin) family of actin binding proteins, which bind to the C-terminal of NHE-RF (27, 31). Other factors, including an extracellular matrix protein named hensin, have also been implicated in generating the plasticity of the intercalated cell phenotype at least *in vitro* (19, 32). An additional interesting finding is that both the B1 and B2 subunits of the H⁺ATPase are capable of binding actin directly via their N-terminal domains (33). Thus, it is possible that the H⁺ATPase interacts with the actin cytoskeleton both directly and indirectly (via NHE-RF). The respective roles and the regulation of these two mechanisms of interaction now need to be evaluated in different cell types. Indeed, phosphorylation of NHE-RF has been shown to disrupt the indirect interaction of the β_2-adrenegric receptor with the actin cytoskeleton and to affect the endocytic sorting of this receptor (34).

Although antibodies against all of the H⁺ATPase subunits were not utilized in this study, at least two major cytosolic subunits associated with the NHE-RF-GST beads in an affinity binding assay, and the E (31 kDa) subunit of the H⁺ATPase was co-immunoprecipitated from rat kidney cytosol by anti-NHE-RF antibodies. Because of interference from the rabbit-derived polyclonal NHE-RF IgG used for immunoprecipitation, we were unable to determine whether the 56-kDa H⁺ATPase subunit was also co-immunoprecipitated from these samples. In addition, our data show that a peptide derived from the C terminus of the B1 56-kDa subunit isoform, but not from the B2 isoform, inhibits interaction of the H⁺ATPase with NHE-RF. Coupled with previous data showing that preassembled H⁺ATPase cytoplasmic domains exist in the cytosol (18), our data suggest that the cytosolic portion of the H⁺ATPase can bind NHE-RF via a specific interaction with the C-terminal DTAL motif that is unique to the B1 subunit. Furthermore, our data provide some evidence that the interaction occurs via the C-terminal domain of the 56-kDa subunit, because the rest of the protein sequence of these two isoforms is similar except for a short N-terminal sequence difference (16, 35). It is likely that when this 56-kDa subunit is assembled in a membrane together with the transmembrane portion of the H⁺ATPase (the Vo sector), the entire H⁺ATPase assembly could thereby be coupled to NHE-RF and thus be anchored into a selected membrane domain. However, it is interesting that this domain can be either the apical or the basolateral domain in the B-intercalated cell. It has been stated recently that NHE-RF expression is restricted to the apical domain of epithelial cells (36), but this is clearly not the case in B-intercalated cells. Thus, NHE-RF may not determine the polarity of H⁺ATPase expression *per se*, but NHE-RF might stabilize the complex once it has reached its target membrane. In other cell types, NHE-RF appears to stabilize the cystic fibrosis transmembrane conductance regulator in the apical plasma membrane (3), whereas in *Caenorhabditis elegans*, PDZ proteins have been proposed to be involved in basolateral anchoring and/or targeting of a TGF-β homolog (37). Recently, a *Drosophila* PDZ protein, discs lost, was also reported to have a dual role in maintaining apical and basolateral epithelial cell polarity (38). However, the diffuse, intracellular pattern of NHE-RF and H⁺ATPase localization seen in some B-intercalated cells raises the possibility that NHE-RF might participate in the trafficking or targeting of the H⁺ATPase. Whether PDZ proteins are involved in anchoring, targeting, or both processes remains to be determined, but our results clearly indicate that this process is not unidirectional (*i.e.* exclusively apical) in every cell type.

In the proximal tubule, NHE-RF is abundant and is colocal-

ized with NHE-3 in the apical brush border (data not shown). This scaffolding interaction is probably responsible for maintaining NHE-3 at a high concentration in the apical membrane (29). The B subunit of the H⁺ATPase that is expressed in this tubule segment lacks the C-terminal DTAL and should be incapable of interacting with PDZ domain proteins (16). Immunofluorescence shows that the H⁺ATPase is not colocalized with NHE-RF at the apical pole of proximal tubules. Because H⁺ATPase is involved in the extensive apical membrane endocytosis and recycling that occurs in proximal tubules (1), it may be advantageous for this cell type to express an isoform of the H⁺ATPase B subunit that cannot interact with NHE-RF at the apical membrane. Such an interaction would anchor the H⁺ATPase in the plasma membrane by cross-linking to the NHE-3/NHE-RF complex and might hinder the endocytotic recycling of this protein, leading to failure of the endosomal acidification process and defective recycling of apical membrane proteins.

We have previously reported that the 56-kDa B1 subunit of the H⁺ATPase is present on endosomes in the other collecting duct cell type, the principal cell (39). These endosomes are involved in recycling the water channel AQP2, they do not acidify their lumen, and they lack other subunits of the H⁺ATPase (39). We postulated that the 56-kDa subunit might be a promiscuous subunit that could associate with the membranes of these endosomes via another, as yet unidentified mechanism. This mechanism can now be envisaged to occur via the PDZ-binding domain, although principal cells were only weakly stained with the anti-NHE-RF antibody. Thus, it is possible that in principal cells, a different PDZ protein such as the NHE-RF related NHE-RF2 (3) might be associated with the 56-kDa H⁺ATPase B1 subunit.

In summary, we have shown that the B1 subunit isoform of the H⁺ATPase is a PDZ-binding protein that associates with NHE-RF and may therefore be responsible for linking the H⁺ATPase to the cytoskeleton in these cells. The two proteins are colocalized in B-intercalated cells but not in A-cells, suggesting a role in generating, maintaining, or modulating the B-cell phenotype. NHE-RF and H⁺ATPase are not colocalized in proximal tubules, which express a truncated B2 subunit isoform of the H⁺ATPase that lacks the PDZ-binding domain.

REFERENCES

1. Brown, D., and Stow, J. L. (1996) *Physiol. Rev.* 76, 245–297
2. Fanning, A. S., and Anderson, J. M. (1998) *Curr. Top. Microbiol. Immunol.* 228, 209–233
3. Hall, R. A., Ostedgaard, L. S., Premont, R. T., Blitzer, J. T., Rahman, N., Welsh, M. J., and Lefkowitz, R. J. (1998) *Proc. Natl. Acad. Sci. U. S. A.* 95, 8496–8501
4. Hall, R. A., Premont, R. T., Chow, C. W., Blitzer, J. T., Pitcher, J. A., Claing, A., Stoffel, R. H., Barak, L. S., Shenolikar, S., Weinman, E. J., Grinstein, S., and Lefkowitz, R. J. (1998) *Nature* 392, 626–630
5. Brenman, J. E., Christopherson, K. S., Craven, S. E., McGee, A. W., and Bredt, D. S. (1996) *J. Neurosci.* 16, 7407–7415
6. Bunn, R. C., Jensen, M. A., and Reed, B. C. (1999) *Mol. Biol. Cell* 10, 819–832
7. Kim, E., Niethammer, M., Rothschild, A., Jan, Y. N., and Sheng, M. (1995) *Nature* 378, 85–88
8. Inanobe, A., Yoshimoto, Y., Horio, Y., Morishige, K. I., Hibino, H., Matsumoto, S., Tokunaga, Y., Maeda, T., Hata, Y., Takai, Y., and Kurachi, Y. (1999) *J. Neurosci.* 19, 1006–1017
9. Burke, N. A., Takimoto, K., Li, D., Han, W., Watkins, S. C., and Levitan, E. S. (1999) *J. Gen. Physiol.* 113, 71–80
10. Wang, S., Raab, R. W., Schatz, P. J., Guggino, W. B., and Li, M. (1998) *FEBS Lett.* 427, 103–108
11. Weinman, E. J., Steplock, D., Wang, Y., and Shenolikar, S. (1995) *J. Clin. Invest.* 95, 2143–2149
12. Weinman, E. J., Steplock, D., Tate, K., Hall, R. A., Spurney, R. F., and Shenolikar, S. (1998) *J. Clin. Invest.* 101, 2199–2206
13. Reczek, D., Berryman, M., and Bretscher, A. (1997) *J. Cell Biol.* 139, 169–179
14. Murthy, A., Gonzalez-Agosti, C., Cordero, E., Pinney, D., Candia, C., Solomon, F., Gusella, J., and Ramesh, V. (1998) *J. Biol. Chem.* 273, 1273–1276
15. Bernardo, A. A., Kear, F. T., Santos, A. V., Ma, J., Steplock, D., Robey, R. B., and Weinman, E. J. (1999) *J. Clin. Invest.* 104, 195–201
16. Nelson, R. D., Guo, X. L., Masood, K., Brown, D., Kalkbrenner, M., and Gluck, S. (1992) *Proc. Natl. Acad. Sci. U. S. A.* 89, 3541–3545
17. Breton, S., Smith, P. J., Lui, B., and Brown, D. (1996) *Nat. Med.* 2, 470–472
18. Nelson, N., and Harvey, W. R. (1999) *Physiol. Rev.* 79, 361–385
19. Al-Awqati, Q. (1996) *Am. J. Physiol.* 270, C1571–C1580
20. Brown, D., Hirsch, S., and Gluck, S. (1988) *Nature* 331, 622–624
21. Alper, S. L., Natale, J., Gluck, S., Lodish, H. F., and Brown, D. (1989) *Proc. Natl. Acad. Sci. U. S. A.* 86, 5429–5433
22. Sabolic, I., Brown, D., Gluck, S. L., and Alper, S. L. (1997) *Kidney Int.* 51, 125–137
23. Purcell, H., Bastani, B., Harris, K. P., Hemken, P., Klahr, S., and Gluck, S. (1991) *Am. J. Physiol.* 261, F365–F376
24. McLean, I. W., and Nakane, P. K. (1974) *J. Histochem. Cytochem.* 22, 1077–1083
25. Breton, S., Alper, S. L., Gluck, S. L., Sly, W. S., Barker, J. E., and Brown, D. (1995) *Am. J. Physiol.* 269, F761–F774
26. Brown, D., Lydon, J., McLaughlin, M., Stuart-Tilley, A., Tyszkowski, R., and Alper, S. (1996) *Histochem. Cell Biol.* 105, 261–267
27. Gonzalez-Agosti, C., Wiederhold, T., Herndon, M. E., Gusella, J., and Ramesh, V. (1999) *J. Biol. Chem.* 274, 34438–34442
28. Alper, S. L., Stuart-Tilley, A. K., Biemesderfer, D., Shmukler, B. E., and Brown, D. (1997) *Am. J. Physiol.* 273, F601–F614
29. Biemesderfer, D., Rutherford, P. A., Nagy, T., Pizzonia, J. H., Abu-Alfa, A. K., and Aronson, P. S. (1997) *Am. J. Physiol.* 273, F289–F299
30. Brown, D., Hirsch, S., and Gluck, S. (1988) *J. Clin. Invest.* 82, 2114–2126
31. Yun, C.-H. C., Lamprecht, G., Forster, D. V., and Sidor, A. (1998) *J. Biol. Chem.* 273, 25856–25863
32. Al-Awqati, Q., Vijayakumar, S., Hikita, C., Chen, J., and Takito, J. (1998) *Am. J. Physiol.* 275, F183–F190
33. Lee, B. S., Gluck, S. L., and Holliday, L. S. (1999) *J. Biol. Chem.* 274, 29164–29171
34. Cao, T. T., Deacon, H. W., Reczek, D., Bretscher, A., and von Zastrow, M. (1999) *Nature* 401, 286–290
35. Puopolo, K., Kumamoto, C., Adachi, I., Magner, R., and Forgac, M. (1992) *J. Biol. Chem.* 267, 3696–3706
36. Fanning, A. S., and Anderson, J. M. (1999) *Curr. Opin. Cell Biol.* 11, 432–439
37. Kim, S. K. (1997) *Curr. Opin. Cell Biol.* 9, 853–859
38. Bhat, M. A., Izaddoost, S., Lu, Y., Cho, K. O., Choi, K. W., and Bellen, H. J. (1999) *Cell* 96, 833–845
39. Sabolic, I., Wuarin, F., Shi, L. B., Verkman, A. S., Ausiello, D. A., Gluck, S., and Brown, D. (1992) *J. Cell Biol.* 119, 111–122

JBC Papers in Press. Published on September 8, 2000 as Manuscript M006635200

Association of Mammalian Trp4 and Phospholipase C Isozymes with a PDZ-Domain-Containing Protein, NHERF

Yufang Tang[1], Jisen Tang[1], Zhangguo Chen[1], Claudia Trost[2], Veit Flockerzi[2], Min Li[3], Vijaya Ramesh[4], Michael X. Zhu[1]

[1]Neurobiotechnology Center, Department of Neuroscience, Ohio State University, Columbus, OH 43210, USA
[2]Institut für Pharmakilogie und Toxikologie der Universität des Saarlandes, D-66421 Homburg, Germany
[3]Department of Physiology and Neuroscience, Johns Hopkins University School of Medicine, Baltimore, MD 21205, USA
[4]Molecular Neurogenetic Unit, Massachusetts General Hospital, Charlestown, MA 02129, USA

Please send all correspondences to:

Michael X. Zhu
The Ohio State University
Neurobiotechnology Center
168 Rightmire Hall
1060 Carmack Road
Columbus, OH 43210
Tel: 614-292-8173
Fax: 614-292-5379
email: zhu.55@osu.edu

Running Title, *Coassembly of Trp4 and PLC with NHERF*

Keyword: Capacitative Ca^{2+} entry, IP_3, Transient Receptor Potential, INAD, Ca^{2+} channel, CCE1.

Summary:

Mammalian homologues of *Drosophila* Trp have been implicated to form channels that are activated following the depletion of Ca^{2+} from internal stores. Recent studies indicate that actin redistribution is required for the activation of these channels. Here we show that murine Trp4 and Trp5, as well as phospholipase C β1 and β2 interact with the first PDZ domain of NHERF, regulatory factor of the Na^+/H^+ exchanger. We demonstrated the association of Trp4 and phospholipase C-β1 with NHERF *in vivo* in an HEK 293 cell line expressing Trp4 and in adult mouse brain by immunocoprecipitation. NHERF is a two PDZ domain-containing protein that associates with the actin cytoskeleton via interactions with members of ezrin/radixin/moesin family. Thus, store-operated channels involving Trp4 and Trp5 can form signaling complexes with phospholipase C isozymes via interactions with NHERF and thereby linking the lipase and the channels to the actin cytoskeleton. The interaction with the PDZ protein may constitute an important mechanism for distribution and regulation of store-operated channels.

Introduction

Ca^{2+} plays very important roles in regulating cell functions ranging from contraction and secretion to proliferation and differentiation. In many cells, stimulation of phospholipase C (PLC) by cell surface receptors is accompanied by an increase in intracellular Ca^{2+} concentrations. This occurs via Ca^{2+} release from internal stores and Ca^{2+} influx from extracellular space (*1,2*). While the mechanism of Ca^{2+} release from the endoplasmic reticulum (ER) is well understood, the channel(s) and mechanism(s) that mediate Ca^{2+} influx remain to be elucidated. It is currently believed that most, if not all, Ca^{2+} influx is mediated through a set of plasma membrane (PM) Ca^{2+}-permeable channels that open in response to internal Ca^{2+} store depletion (*3,4*). These channels are referred to as store-operated channels (SOCs). Molecular cloning and functional expression have revealed that the products of the *Drosophila transient receptor potential (trp)* gene as well as a number of its mammalian homologues form SOCs (*5-11*). Other Trp homologues form Ca^{2+}-permeable cation channels that do not appear to be store-operated (*12-16*), as they do not respond to treatment by thapsigargin, an intracellular Ca^{2+}-ATPase inhibitor that induces passive store-depletion by preventing the reuptake of Ca^{2+} to the ER. However, in all cases, the Trp-formed channels are activated by signaling events down-stream from receptor activation and PLC stimulation. Moreover, a store depletion-insensitive Trp subunit may heteromultimerize with a store depletion-sensitive Trp to form a SOC (*17, 18*). Therefore, store-operated Ca^{2+} influx is most likely mediated by channels formed by Trp proteins.

In *Drosophila* eyes, Trp is organized in a supramolecular complex along with other phototransduction proteins, such as PLC and protein kinase C (PKC), through association with a multi-PDZ domain containing protein, INAD (inactivation no after potential D) (*19-21*). PDZ

domains were first identified as 80 ~100 amino acid repeated sequences in the neuron-specific post-synaptic density protein (PSD-95/SAP-90), the *Drosophila* septate junction protein disk-large (dlg) and the epithelial tight-junction protein zona occludens-1 (ZO1) (*22*). Growing evidence suggests that these domains are important protein-protein interaction sites for clustering and organization of signaling molecules, particularly those involved in ion transport (*22-24*). INAD contains five PDZ domains, each of which interacts with a particular target protein and thus serves as a scaffold to bring PLC, Trp, PKC and G protein together in a signaling complex. Although INAD is not directly involved in transmitting the signal of light perception, it plays a critical role in localizing PLC and Trp at the proper sites of the rhabdomere of *Drosophila* photoreceptors (*19,20*). Since PLC-mediated signaling in mammals is very similar to phototransduction cascade of insects, an INAD-like scaffold may exist in mammalian cells. Although several multi-PDZ domain-containing proteins distantly related to INAD have been cloned from human and rodents (*25-27*), none has been shown to interact with mammalian Trp or PLC.

The interaction between a target protein and a specific PDZ domain is often determined by the last three C-terminal residues of the target (*28*). Because the C-terminal sequences of mammalian Trps are very different from their *Drosophila* counterpart and also very diverse among themselves (Fig. 1*a*), each Trp may bind to different PDZ domains and the PDZ domains that bind to the mammalian Trps may be quite different from that of INAD. Here we show that murine Trp4 (mTrp4) and Trp5 bind to the first PDZ domain of the Na^+-H^+ exchanger regulatory factor (NHERF). We additionally show that the same PDZ domain binds to the C-termini of PLCβ1 and PLCβ2, indicating that NHERF is capable of bringing together the signaling molecules involved in the PLC-mediated pathway in mammalian cells and therefore, may play a

role similar to that of INAD in insect phototransduction. We demonstrate the physical association of PLCβ1, Trp4 and NHERF in an HEK 293 cell line stably expressing mTrp4 and in adult mouse brain by immunocoprecipitation experiments.

Experimental Procedures

Materials: Phenylmethanesulfonyl fluoride, benzamide, aprotinin, soybean trypsin inhibitor, and leupeptin were purchased from Sigma. Nitrocellulose membranes and protein markers were purchased from Bio-Rad. Protein A-Sepharose (4 Fast Flow), glutathione Sepharose 4B, and Enhanced Chemiluminescence (ECL) detection system were purchased from Amersham/Pharmacia Biotech. TNT (transcription and translation) coupled rabbit reticulocyte lysate system was from Promega. ^{35}S-expressed protein labeling mix (11 Ci/Liter) was from NEN Life Science Products. Lubrol and IGEPAL were obtained from ICN Biochemicals. Dulbecco's modified Eagle's medium (DMEM), fetal bovine serum, penicillin/streptomycin, trypsin-EDTA were purchased from Life Technologies. All other chemicals were from Fisher Scientifics.

Antibodies: The rabbit polyclonal anti-NHERF antibody IC270 was raised against the C-terminal synthetic peptide of human NHERF as described previously (*29*). A rabbit polyclonal anti-Trp4 antibody, T4cAb, was raised against a synthetic peptide representing the last 13 residues of bovine Trp4 as described (*30*). Another rabbit polyclonal anti-Trp4 antibody, T4nAb, was raised against the synthetic Trp4 N-terminal peptide, CYYKRNVNAPYRDR (Quality Controlled Biochemicals, Hopkinton, MA, USA). The rabbit polyclonal antibodies for PLCβ1 (G-12) and HisTag (H-15) were from Santa Cruz Biotechnologies (Santa Cruz, CA).

The monoclonal antibody 12CA5 for hemagglutinin (HA) epitope was from Babco (Berkeley, CA).

cDNAs and Expression Constructs: Full-length cDNAs for murine Trp4 and Trp5 was obtained from a mouse brain cDNA library for rapid amplification of complimentary ends by polymerase chain reaction (RACE-PCR) made according to the protocol provided by the Marathon cDNA Amplification kit (Clontech). RACE-PCR primers were designed and the reactions were carried out following the previous description (*7*). DNA sequences were determined by the dideoxy-chain termination method (*31*). The sequences for murine Trp4α, Trp4β and Trp5 have been deposited in GenBank database with accession numbers AF011543, AF019663, and AF060107, respectively. For in vitro synthesis of ^{35}S-labeled proteins, the cDNAs were subcloned into the expression vector pAGA (*32*), which contains a T7 promoter that allows transcription initiation by T7 RNA polymerase. An ATG codon contained within an NcoI site serves as a translation initiation site. The C-terminal constructs for Trp4α and Trp5 were made by subcloning HindIII/EcoRI fragments encoding the corresponding sequences into pAGA at the NcoI site via blunt-end ligation after each fragment had been filled-in by the Klenow fragment of DNA polymerase I in the presence of dNTP. cDNAs for bovine PLCβ1 and PLCβ2 were kindly provided by Dr. Peter Gierschik. Their C-terminal constructs were made by subcloning a PvuII/BamHI fragment of PLCβ1 or a PvuII/XbaI fragment of PLCβ2 into pAGA at the NcoI site via blunt-end ligation. HA-tagged *trp4* constructs contain the coding nucleotide sequence for the HA epitope, "YPYDVPDY", immediately after the coding sequence for the C-terminal end of Trp4 "VTTRL". A stop codon was added after the codon for the last "Y" of the HA-epitope. For expression in HEK 293 cells, the cDNA for the full-length mTrp4α or the C-

terminal HA-tagged mTrp4α was subcloned into pcDNA3 (Invitrogen). Constructs for preparing glutathione S transferase (GST) fusion proteins for PDZ1 and PDZ2 of NHERF were as described (*28*).

GST Pull-down experiments: GST and GST-fusion proteins were produced in *E. coli* BL-21 cells after transformation with corresponding plasmids. Synthesis of recombinant proteins was induced by the addition of 100 μM isopropyl-1-thio-D-galactopyranoside to log-phase cultures (A600 = ~0.6) at 37°C. After 3-5 hrs of incubation with constant shaking, the bacteria were recovered by centrifugation at 4°C for 15 min and either used immediately or stored at -20°C. GST and GST-fusion proteins were purified, using glutathione Sepharose 4B, from bacterial lysates prepared by incubating with 20 mM lysozyme and 1% sarcosyl and sonication. The glutathione beads with the bound proteins were washed three times with washing buffer (20 mM Tris-Cl, pH 8.0, 1 mM EDTA, 150 mM NaCl, 0.5% IGEPAL) and then resuspended in a binding buffer containing 20 mM Tris-Cl, pH 8.0, 100 mM KCl, 2 mM $MgCl_2$ and 0.5% Lubrol. ^{35}S-labeled Trp4, Trp5, or the C-terminal portions of Trp4, Trp5, PLCβ1, and PLCβ2 were made *in vitro* using the TNT coupled rabbit reticulocyte system. GST protein (2 μg) bound to glutathione Sepharose and 10 μl ^{35}S-labeled protein were added to 250 μl of the binding buffer and were incubated on a platform shaker at room temperature for 30 min. The bound proteins were collected by centrifugation at 5,000 rpm for 2 min and washed three times with the binding buffer. After the last wash, 10 μl 2 X Laemmli buffer (1 X = 62.5 mM Tris-Cl, 1% SDS, 10% glycerol, 10% β-mercaptoethanol, pH 6.8) was added to the pellet and the samples were incubated at room temperature for 5 min. Aliquots (10 μl) of each sample were subjected to

SDS-PAGE and the gels were stained with Coomassie blue, dried and exposed to X-ray films overnight.

Cell lines and Cell Culture: HEK293 cells were grown in DMEM containing 4.5 mg/ml glucose, 10% heat-inactivated fetal bovine serum, 50 units/ml penicillin, and 50 μg/ml streptomycin. For transfection, 2.8 x 10^6 cells were cultured in a 10 cm tissue culture dish for 20 hrs and 5 μg m*trp4α*/pcDNA3 or m*trp4α-HAc*/pcDNA3 was transfected into the cells by the calcium phosphate precipitation method as described (*34*). After 24 hours, cells were harvested, suspended in the same medium supplemented with 400 μg/ml G418, and transferred to wells of 96-well plates in three serial dilutions of 1:4. G418-resistant transformants that appeared to arise from single colonies were transferred to 12-well plates for growth and further analysis. Clonal cell lines expressing Trp4α or C-terminal HA-tagged Trp4α were identified by immunocytochemistry and confirmed by immunoprecipitation as detailed before (*34*) using an affinity purified polyclonal anti-Trp4 N-terminal antibody, T4nAb. The stable cell lines were diluted twice weekly and maintained in medium supplemented with 400 μg/ml G418.

Immunocoprecipitation and immunoblotting: HEK 293 cells were washed twice in phosphate-buffered saline (PBS: 136 mM NaCl, 1.4 mM KCl, 10 mM Na_2HPO_4, 1.7 mM KH_2PO_4, pH 7.4), scraped off from the dishes in 1 ml of ice-cold PBS supplemented with protease inhibitors (0.1 mM phenylmethylsulfonyl fluoride, 1 mM benzamide, 1 μg/ml aprotinin, 10 μM leupeptin, 1 μM Soybean protease inhibitor), and pelleted by centrifugation at 5,000 rpm in a microcentrifuge at 4°C for 2 min. Cells were sonicated in RIPA buffer containing 150 mM NaCl, 50 mM Tris-Cl, pH 8.0, 0.5% sodium deoxycholate, 1% IGEPAL, 0.1% SDS, 5 mM

EDTA and the protease inhibitors listed above. Mouse brain samples were homogenized using a polytron homogenizer in 1 ml RIPA buffer containing protease inhibitors followed by sonication. All procedures for immunoprecipitation were carried out at 4°C. The crude lysate was centrifuged at 14,000 rpm in a microcentrifuge for 10 min and the supernatant was transferred to a new Eppendorf tube. Non-specific bindings were removed by a preincubation with 1/10 volume of protein-A Sepharose for 1 h followed by a low speed centrifugation at 5,000 rpm for 2 min. The supernatant was then incubated with appropriate dilutions of the desired antibody for 10-16 hrs. The dilutions for the antibodies were 1:200 for anti-Trp4, 1:100 for anti-NHERF and anti-PLCβ1. Immuncomplexes were purified by incubation with 1/10 volume of protein-A-Sepharose for 1 h, centrifuged and washed three times in RIPA buffer. Bound immuncomplexes were eluted by incubating the Sepharose beads in 50 µl 2 X Laemmli buffer at 95°C for 10 min. The samples were centrifuged briefly at 14,000 rpm and 10 µl aliquot of the supernatant was subjected to SDS-PAGE. The proteins were then transferred to nitrocellulose membranes using a Semi-dry Transfer Blotter (W. E. P. co, Concord, CA) at 120 mA for 2 hrs and immunoblotted with antibodies as indicated. For immunoblotting, dilutions of antibodies were 1:2,000 for anti-Trp4, 1:1,000 for anti-NHERF and anti-PLCβ1. Horse radish peroxidase conjugated goat anti-rabbit IgG was used as secondary antibody and all blots were developed using the ECL system.

Results

Among the seven mammalian Trp homologues currently known, Trp4 and Trp5 are the most closely related. The first 754 residues of mTrp4, encompassing the N-terminus, the transmembrane regions, and the first 133 residues of the C-terminus, share 73% identity (82% similarity) with the equivalent regions of mTrp5 (761 residues). However, the last 220 residues

of Trp4 are divergent from the last 214 residues of Trp5 with an identity score of 20% and a similarity score of 38%. Strikingly, both proteins end with the same C-terminal sequence, "VTTRL" (Fig. 1*a*). Since the ligand specificities of PDZ domains are often defined by the last few residues of target proteins, this sequence conservation suggests that Trp4 and Trp5 might interact with a common PDZ-domain. Random peptide library screening has revealed that peptides terminating with the amino acid sequence "TRL" bound with high affinity to the first PDZ domain of NHERF (*28*). Therefore, we tested whether Trp4 and Trp5 interact with NHERF in GST pull-down experiments. Fig. 1*b* shows that the GST fusion protein containing PDZ1 of NHERF interacted with ^{35}S-labeled full-length mTrp4 and mTrp5. PDZ2 of NHERF interacted with Trp4 and Trp5 only very weakly. In agreement with the notion that the C-terminal sequences of the target proteins are responsible for the interaction with PDZ domains, NHERF PDZ1 also interacted with the C-terminal portions of Trp4 or Trp5 (Fig. 1*c*). In contrast, human Trp3 terminates with "MLRCE" and did not interact with NHERF PDZ1 (Fig. 1*d*). Molecular cloning has revealed the existence of at least two forms of mTrp4: a longer form (Trp4α) that contains 974 amino acids and a shorter form (Trp4β) that contains 890 amino acids and lacks residues 781-864 corresponding to Trp4α. Because the C-terminal ends remain the same, both Trp4α and Trp4β interact with PDZ1 of NHERF (Fig. 1*e*). However, when the C-terminus was masked by the addition of an HA epitope, neither Trp4 isoform interacted with NHERF (Fig. 1*e*). These data indicate that the presence of "TRL" motif at the C-terminal end is essential for the interaction between Trp4 and NHERF PDZ1.

While the "VTTRL" sequence is found at the C-terminal end of bovine, human and murine Trp4, it has been reported that rat Trp4 terminates with "HKIMI" (GenBank Accession number: AB008889). In order to confirm this, we isolated total RNA from the brain of an adult

Sprague-Dawley rat and performed RT-PCR using primers that would anneal to both mouse and rat *trp4*. Products corresponding to *trp4α* and *trp4β* were obtained and sequenced. Despite of the 99.4% identity with the published rat *trp4* (AB008889) at the nucleotide level, our PCR products predict proteins with "VTTRL" at the C-termini (GenBank Accession numbers: AF288407, AF288408). Therefore, the "VTTRL" sequence and hence the association with NHERF is conserved among Trp4 orthologues in mammalian species.

Bovine PLCβ1 and PLCβ2 terminate with "TPL" and "SRL", respectively (Fig. 2*a*). Results of the random peptide library screening (*28*) indicated that these sequences might also interact with PDZ1 of NHERF. Therefore, we tested the binding of PLCβ1 and PLCβ2 with the two PDZ domains of NHERF. As shown in Fig. 2*b*, ^{35}S-labeled C-terminal fragments of PLCβ1 and PLCβ2 bound to GST-fusion protein containing PDZ1 but only very weakly to that containing PDZ2 of NHERF. Thus, the first PDZ domain of NHERF is capable of interacting with PLCβ1, PLCβ2, Trp4, and Trp5, suggesting that NHERF may serve as a scaffold for the clustering of PLC signaling molecules in mammalian cells.

In order to test whether Trp4 associates with NHERF *in vivo*, we expressed mTrp4α in HEK 293 cells and established a stable cell line, T4-60. In immunoblotting, a rabbit polyclonal antibody (T4cAb) raised against a peptide representing the last 13 amino acids of Trp4 (*30*) recognized a 110 kDa polypeptide in membranes prepared from T4-60 cells but not that from either untransfected HEK cells or a cell line stably expressing human Trp3 (Fig. 3*a*). The expression of endogenous NHERF in HEK 293 cells was detected in total cell lysates using an anti-NHERF specific antibody, IC270 (Fig. 3*b*). Moreover, the association of Trp4 with NHERF was examined by first immunoprecipitating cell extracts using IC270 followed by the separation of precipitated proteins by SDS-PAGE and immunoblotting using the anti-Trp4, T4cAb. Trp4

was detected in the precipitates obtained from T4-60 but not untransfected cells (Fig. 3*c*). No Trp4 signal was found in the blot made from immunoprecitipation of T4-60 cell lysate using a non-specific antibody, anti-HA 12CA5 (not shown). In addition, an anti-Trp4 N-terminal antibody (T4nAb) also detected Trp4α in the anti-NHERF immunoprecipitates from the T4-60 cells but not from cells expressing Trp3 or the C-terminal-tagged Trp4α (Fig. 3*c*). The expression of the HA-tagged Trp4α in this cell line was confirmed by immunoprecipitation with T4nAb followed by immunoblotting with the anti-HA antibody. These data demonstrated that Trp4 interacts with NHERF *in vivo* and that the presence of "TRL" at the C-terminal end of Trp4 is essential for this interaction.

Endogenous PLCβ1 can be detected in HEK 293 cells using a polyclonal anti-PLCβ1 antibody (Fig. 4*a*). Immunoblotting with the antibody revealed the presence of PLCβ1 in immunoprecipitates obtained using the anti-NHERF antibody (Fig. 4*b*) and thereby demonstrating that endogenous PLCβ1 and NHERF associate with each other *in vivo* in HEK 293 cells. Moreover, in T4-60 cells, PLCβ1 coprecipitated with Trp4 in immunoprecipitates obtained using the anti-Trp4 antibody (Fig. 4*b*). Interestingly, the amount of PLCβ1 coprecipitated by the anti-Trp4 antibody was similar to that precipitated by the anti-NHERF antibody (Fig. 4*b*). Assuming that the two antibodies had the same efficiency for the precipitation of the NHERF/Trp4 complex, this result indicates that most likely, PLCβ1 is part of the same complex that contains Trp4 and NHERF. Thus, the three proteins appear to coassemble in HEK cells expressing Trp4.

In order to determine whether the three proteins also coassemble in animal tissues that normally express them, we performed immunocoprecipitation experiments using adult mouse brain. Significant amounts of PLCβ1 and NHERF were detected in mouse brain by

immunoblotting using the respective specific antibodies (Fig. 5*a,* left and middle). The expression of Trp4 in adult mouse brain was difficult to detect by immunoblotting alone using the anti-Trp4, T4cAb. However, two bands, 110 kDa and 100 kDa, presumably representing the α and β isoforms of Trp4, were detected by immunoprecipitation followed by immunoblotting using the same antibody (Fig. 5*a,* right). Immunocoprecipitation experiments showed that the anti-NHERF antibody also precipitated the two isoforms of Trp4 from the brain lysate (Fig. 5*b*) and that similar amount of PLCβ1 was precipitated by the anti-NHERF, IC270 and the anti-Trp4, T4cAb (Fig. 5*c*). An unrelated rabbit polyclonal antibody, anti-HisTag, did not precipitate Trp4 or PLCβ1. Thus, PLCβ1, Trp4, and NHERF coexist as a molecular complex in adult mouse brain.

Discussion:

Our data suggest that NHERF is a molecular scaffold that brings PLC isozymes and Trp4 or Trp5 into a signaling complex. Similar function is known to be carried out by INAD in the *Drosophila* phototransduction system (*19-21*). The association with INAD appears to be crucial for the proper localization of the cascading enzymes as well as for the precision of the spatial and temporal control of signaling events, such as those involved in the recruitment of G protein upon stimulation (*38*) and the inactivation of Trp by PKC-mediated phosphorylation (*39,40*). NHERF was first isolated as a cofactor required for protein kinase A-mediated inhibition of type 3 Na^+-H^+ exchanger found on the renal brush border membrane (*41,42*) and later determined to be the same as the phosphoprotein that binds members of the ezrin/radixin/moesin (ERM) proteins (*33,43*). The ERM proteins are known to link cell surface receptors to actin cytoskeleton (*44*) and in many case such link is mediated through NHERF. The two PDZ domains of NHERF bind to target proteins while its C-terminus binds to the N-terminus of ERMs (*33, 43*). It has been shown that the first PDZ-domain of NHERF interacts with a number of G-protein-coupled receptors and ion transporting proteins, such as the cystic fibrosis transmembrane conductance regulator (CFTR), sodium-bicarbonate transporters, and H^+-ATPase (*28,45-48*). Analysis of the sequence requirement for NHERF PDZ1 binding also suggested PLCβ1 as a potential ligand (*45*). Indeed, we show here that the C-termini of both PLCβ1 and PLCβ2 bind NHERF PDZ1. In addition, this PDZ domain also binds Trp4 and Trp5. Our immunocoprecipitation studies further demonstrated the association of PLCβ1, Trp4, and NHERF in the same complex in HEK 293 cells expressing mTrp4 and in mouse brain. Because the ligand specificity of PDZ domain interaction is determined, in most cases, by the last 3 to 4 C-terminal amino acids of the target proteins, it is predictable that only a subset of mammalian Trps can interact directly with

NHERF. Thus, NHERF is considered one of the functional analogs of INAD. Several other PDZ-domain-containing proteins may exist for the clustering of other Trps.

There are differences between NHERF and INAD. First, INAD has five PDZ-domains with PLCβ binding to PDZ1 and PDZ5 (*19,21*) whereas Trp binds to PDZ3 (*19*). In contrast, NHERF has only two PDZ domains and PLCβ1/2 and Trp4/5 all bind to PDZ1. It is thus unlikely that a single NHERF molecule binds simultaneously to PLCs and Trps. Rather, it is possible that the molecules are clustered via NHERF's self-association (*49*) or its association with ERMs, which oligomerize among themselves (*44,50*). In such a case, the stoichiometry for PLCβ, NHERF and Trp4 in the molecular complexes may vary greatly. Second, unlike INAD, which is photoreceptor-specific protein primarily involved in scaffolding and modulating the photosensing signaling molecules, NHERF appears to participate in multiple signaling pathways, as shown by its interaction with multiple types of receptors, ion channels, transporters and exchangers. Therefore, questions remain as to how NHERF selects among its many potential partners and what the physiological significance of each association is. The answer to the first question may lie partly on the tissue-specific distribution of each target protein. However, in the case of PLCβ and Trp4, some kind of sorting mechanism would have to be incorporated so that the binding with one partner does not overwhelm the association with the others. For the second question, although the specific physiological implication for each association is not known, there are functions that may be common to all target proteins. These include preferential distribution to the apical membrane of polarized cells (*51,52*), facilitation of phosphorylation by protein kinase A (*53*), which associates with ERM (*54*), and by non-receptor tyrosine kinase, *e. g.* c-Yes, through interaction of NHERF PDZ2 with Yes-associated protein 65 (*51*).

It was recently shown that actin redistribution plays a critical role in activating SOCs in cultured smooth muscle cells and HEK 293 cells as well as in activating Trp3 expressed in the HEK cells (*55,56*). The binding of Trp4 (and Trp5) to NHERF constitutes the first physical link of these channels to actin cytoskeleton. The C-terminus of NHERF interacts with the N-terminus of ezrin, moesin (*43*) and the related protein merlin (*33*). The C-terminus of ERM protein interacts with F-actin in a manner that is dependent on the oligomerization and the phosphorylation states of ERM (*44,57,58*). Blocking ERM dephosphorylation by the phosphatase inhibitor, calyculin A, led to condensation of F-actin in the cell periphery (*59*) and inhibition of SOCs (*56*). Conceivably, the phosphorylation state of ERMs will also affect the dynamics of association of Trp4/5 with actin network due to their association with ERMs via NHERF. Thus, physical association of SOCs with ERM proteins may be one of the reasons that capacitative Ca^{2+} entry is dependent on the reversible redistribution of actin and is blocked by phosphatase inhibitors (*55,56*). Other Trp proteins may multimerize with Trp4 or Trp5 and hence associate with ERMs. Although Trp4 has been shown to be a part of native SOCs in adrenal cells (*30*), it is yet to be established Trp4 or Trp5 also participate in the formation of SOCs in other cell types. Perhaps in the absence of Trp4/5, different PDZ domain-containing proteins are involved in linking the channels to the ERMs through a similar mechanism.

Abbreviations: BSA, bovine serum albumin; DMEM, Dulbecco's modified Eagle's medium; ECL, Enhanced Chemiluminescence; ER, endoplasmic reticulum; ERM, ezrin/radixin/moesin; GST, glutathione S transferase; HA, hemagglutinin; INAD, inactivation no after potential D; mTrp4, murine Trp4; NHERF, Na^+/H^+ exchanger regulatory factor; PBS, phosphate-buffered saline; PDZ, PSD95/DLG/ZO-1; PKC, protein kinase C; PLC, phospholipase C; PM, plasma

membrane; RACE-PCR, rapid amplification of complimentary ends by polymerase chain reaction; SOC, store-operated channel; Trp, transient receptor potential.

Acknowledgement--We thank Dr. P. Gierschik for the cDNAs for bovine PLCβ1 and PLCβ2, Ms. D. Chuang for technical assistance, Dr. P. E. Kolattukudy and A. Young for critical reading and helpful discussions of the manuscript. The work is supported in part by NIH grant GM54235 to M.X.Z. and by a U.S. Army grant to V.R.

References:

1. Putney, J.W. Jr. (1990) *Cell Calcium* **11**, 611-624

2. Berridge, M. J. (1995) *Biochem. J.* **312**, 1-11

3. Fasolato, C., Innocenti, B., and Pozzan, T. (1994) *Trends in Pharmac. Sci.* **15**, 77-83

4. Clapham, D.E. (1995) *Cell* **80**, 259-268

5. Vaca, L., Sinkins, W.G., Hu, Y., Kunze, D.L., and Schilling, W.P. (1994) *Am. J. Physiol.* **267**, C1501-C1505

6. Petersen, C.C.H., Berridge, M.J., Borgese, F., and Bennet, D.L. (1995) *Biochem. J.* **311**, 41-44

7. Zhu, X., Jiang, M., Peyton,M., Boulay,G., Hurst, R., Stefani, E. and Birnbaumer, L. (1996) *Cell* **85**, 661-671

8. Philipp, S., Cavalie, A., Freichel, M., Wissenbach, U., Zimmer, S., Trost, C., Marquart, A., Murakami, M., and Flockerzi, V. (1996) *EMBO J.* **15**, 6166-6171

9. Zitt, C., Zobel, A., Obukhov, A. G., Harteneck, C., Kalkbrenner, F., Luckhoff, A., and Schultz, G. (1996) *Neuron* **16**, 1189-1196

10. Philipp, S., Hambrecht, J., Braslavski, L., Schroth, G., Freichel, M., Murakami, M., Cavalie, A., and Flockerzi, V. (1998) *EMBO J.* **17**, 4274-4282

11. Vannier, B., Peyton, M., Boulay, G., Brown, D., Qin, N., Jiang, M., Zhu, X., and Birnbaumer, L. (1999) *Proc. Natl. Acad. Sci. U. S. A.* **96**, 2060-2064

12. Hu, Y., Vaca, L., Zhu, X., Birnbaumer, L., Kunze, D.L., and Schilling, W.P. (1994) *Biochem. Biophys. Res. Commun.* 201, 1050-1056

13. Boulay, G., Zhu, X., Peyton, M., Jiang, M., Hurst, R. Stefani, E. and Birnbaumer, L. (1997) *J. Biol. Chem.* **272**, 29672-29680

14. Zitt, C., Obukhov, A.G., Strubing, C., Zobel, A., Kalkbrenner, F., Luckhoff, A., and Schultz, G. (1997) *J. Cell Biol.* **138**, 1333-1341

15. Okada, T., Shimizu, S., Wakamori, M., Maeda, A., Kurosaki, T., Takada, N., Imoto, K., and Mori, Y. (1998) *J. Biol. Chem.* **273**, 10279-10287

16. Okada, T, Inoue, R., Yamazaki, K., Maeda, A., Kurosaki, T., Yamakuni, T., Tanaka, I., Shimizu, S., Ikenaka, K., Imoto, K., and Mori, Y. (1999) *J. Biol. Chem.* **274**, 27359-27370

17. Gillo, B., Chorna, I., Cohen, H., Cook, B., Manistersky, I., Chorev, M., Arnon, A., Pollock, J.A., Selinger, Z., and Minke, B. (1996) *Proc. Natl. Acad. Sci. U. S. A.* **93**, 14146-14151

18. Xu, X.Z., Li, H.S., Guggino, W.B., and Montell, C. (1997) *Cell* **89**, 1155-1164

19. Tsunoda, S., Sierralta, J., Sun, Y., Bodner, R., Suzuki, E., Becker, A., Socolich, M., and Zuker, C.S. (1997) *Nature* **388**, 243-249

20. Chevesich, J., Kreuz, A.J., and Montell, C. (1997) *Neuron* **18**, 95-105

21. van Huizen, R., Miller, K., Chen, D.M., Li, Y., Lai, Z.C., Raab, R.W., Stark, W.S., Shortridge, R.D., and Li, M. (1998) *EMBO J.* **17**, 2285-2297

22. Fanning, A.S. and Anderson, J.M. (1996) *Curr. Biol.* **6**, 1385-1388

23. Pawson, T. and Scott, J.D. (1997) *Science,* 278, 2075-2080

24. Craven, S.E. and Bredt, D.S. (1998) *Cell* **93**, 495-498

25. Philipp, S. and Flockerzi, V. (1997) *FEBS Lett.* **413**, 243-248

26. Ullmer, C., Schmuck, K., Figge, A., and Lubbert, H. (1998) *FEBS Lett.* **424**, 63-68

27. Kurschner, C., Mermelstein, P.G., Holden, W.T., and Surmeier, D.J. (1998) *Mol. Cell Neurosci.* **11**, 161-172

28. Wang, S., Raab, R.W., Schatz, P.J, Guggino, W.B., and Li, M. (1998) *FEBS Lett.* **427**, 103-108

44. Bretscher, A., Reczek, D., and Berryman, M. (1997) *J. Cell Sci.* **110**, 3011-3018

29. Gonzalez-Agosti, C., Wiederhold, T., Herndon, M.E., Gusella, J., and Ramesh, V. (1999) *J. Biol. Chem.* **274**, 34438-34442

30. Philipp, S., Trost, C., Warnat, J., Rautmann, J., Himmerkus, N., Schroth, G., Kretz, O., Nastainczyk, W., Cavalie, A., Hoth, M., and Flockerzi, V. (2000) *J. Biol. Chem.* **275**, 23965-23972

31. Sanger, F., Nicklen, S., and Coulson, A.R. (1977) *Proc. Natl. Acad. Sci. U. S. A.* **74**, 5463-5467

32. Sanford, J., Codina, J., and Birnbaumer, L. (1991) *J. Biol. Chem.* **266**, 9570-9579

33. Murthy, A., Gonzalez-Agosti, C., Cordero, E., Pinney, D., Candia, C., Solomon, F., Gusella, J., and Ramesh, V. (1998) *J. Biol. Chem.* **273**, 1273-1276

34. Zhu, X., Jiang, M. and Birnbaumer, L. (1998) *J. Biol. Chem.* **273**, 133-142

35. Shieh, B.H. and Zhu, M.Y. (1996) *Neuron* **16**, 991-998

36. Levy, F.O., Zhu, X., Kaumann, A.J., and Birnbaumer, L. (1993) *Proc. Natl. Acad. Sci. U. S. A.* **90**, 10798-10802

37. Dare, E., Kifor, O., Brown, E.M., and Weber, G. (1998) *J. Mol. Endocrinol.* **21**, 7-17

38. Bahner, M., Sander, P., Paulsen, R., and Huber, A. (2000) *J. Biol. Chem.* **275**, 2901-2904

39. Huber, A., Sander, P., Bahner, M., and Paulsen, R. (1998) *FEBS Lett.* **425**, 317-322

40. Liu, M., Parker, L.L., Wadzinski, B.E., and Shieh, B.H. (2000) *J. Biol. Chem* **275**, 12194-12199

41. Weinman, E.J., Steplock, D., Wang, Y., and Shenolikar, S. (1995) *J. Clin. Invest.* **95**, 2143-2149

42. Yun, C.H., Oh, S., Zizak, M., Steplock, D., Tsao, S., Tse, C.M., Weinman, E.J., and Donowitz, M. (1997) *Proc. Natl. Acad. Sci. U. S. A.* **94**, 3010-3015

43. Reczek, D., Berryman, M., and Bretscher, A. (1997) *J. Cell Biol.* **139**, 169-179

45. Hall, R.A., Ostedgaard, L.S., Premont, R.T., Blitzer, J.T., Rahman, N., Welsh, M.J., Lefkowitz, R.J. (1998) *Proc. Natl. Acad. Sci. U. S. A.* **95**, 8496-8501

46. Hall, R.A., Premont, R.T., Chow, C.W., Blitzer, J.T., Pitcher, J.A., Claing, A., Stoffel, R.H., Barak, L.S., Shenolikar, S., Weinman, E.J., Grinstein, S., and Lefkowitz, R.J. (1998) *Nature* **392**, 626-630

47. Minkoff, C., Shenolikar, S., and Weinman, E.J. (1999) *Curr. Opin. Nephrol. Hypertens.* **8**, 603-608

48. Breton, S., Wiederhold, T., Marshansky, V., Nsumu, N.N., Ramesh, V., and Brown D. (2000) *J. Biol. Chem.* **275**, 18519-18224

49. Fouassier, L., Yun, C.C., Fitz, J.G., and Doctor, R.B. (2000) *J. Biol. Chem.* **275**, *in press*

50. Tsukita, S., Yonemura, S., and Tsukita, S. (1997) *Trends Biochem. Sci.* **22**, 53-58

51. Mohler, P.J., Kreda, S.M., Boucher, R.C., Sudol, M., Stutts, M.J., Milgram, S.L. (1999) *J. Cell Biol.* **147**, 879-890

THIS PAGE LEFT BLANK INTENTIONALLY

Legend to Figures

Figure 1. Trp4 and Trp5 interact with the first PDZ domain of NHERF. *a*, C-terminal sequences of *Drosophila* Trp, Trp-like and the seven mammalian Trp homologues. Shown are the last 15 residues for each Trp. Except for the last five amino acids (underlined) of Trp4 and Trp5, the C-termini of Trp proteins are not conserved. Double underlined sequence in *Drosophila* Trp had been shown to be critical for the interaction between the Trp and INAD (*35*). *b*, interaction of full-length Trp4 and Trp5 with PDZ domains of NHERF. ^{35}S-labeled mTrp4 and mTrp5 were incubated with GST or GST fusion of NHERF PDZ1 or PDZ2 bound to glutathione Sepharose and bound proteins were separated by SDS-PAGE (8%) as described in the Experimental Procedures. *c*, interaction of the C-terminal portions of Trp4 and Trp5 with NHERF PDZ domains. The ^{35}S-labeled proteins contained portions of mTrp4 and mTrp5 as indicated by the positions of the amino acids shown in parentheses. Proteins were separated by 12% SDS-PAGE. *d*, NHERF PDZ1 interacts with Trp4, Trp5, but not Trp3. *e*, NEHRF PDZ1 interacts with Trp4α and Trp4β but not C-terminal HA-tagged Trp4 isoforms. Experiments were performed as in *b*. For *b-e*, upper panels show autoradiograms of input ^{35}S-labeled proteins and those retained by GST-fusion proteins. Lower panels show the amount of GST or GST-fusion proteins used as revealed by Commassie blue staining. Sizes (in kD) of molecular weight markers are indicated to the left. Lane labels in *b, c, e*: L, total lysate; G, GST; 1, GST-NHERF PDZ1; 2, GST-NHERF PDZ2.

Figure 2. PLCβ1 and PLCβ2 interact with the first PDZ domain of NHERF. *a*, C-terminal sequences of bovine PLCβ1 and PLCβ2. Shown are the last 15 residues for each protein. *b*, Interaction of PLCβ1 and PLCβ2 with PDZ domains of NHERF. ^{35}S-labeled C-terminal

portions of PLCβ1 and PLCβ2 were incubated with GST or GST fusion of NHERF PDZ1 or PDZ2 bound to glutathione Sepharose and bound proteins were separated by 12% SDS-PAGE. Upper panel shows the autoradiogram of input ^{35}S-labled proteins and those retained by GST-fusion proteins. Lower panel shows the amount of GST or GST-fusion proteins used as revealed by Commassie blue staining. Molecular weights are indicated to the left.

Figure 3. Interaction of Trp4 with endogenous NHERF in HEK 293 cells expressing mTrp4α. *a,* expression of Trp4 was detected in T4-60 (T4) but not untransfected control (C) or Trp3 transfected (T3) cells by immunoblotting using the anti-Trp4 C-terminal antibody, T4cAb. Crude membrane preparations were made according to Levy et al (*36*) and 2 μg total protein was used in each lane. *b,* NHERF was detected in control and T4-60 cells by immunoblotting using the anti-NHERF antibody, IC270. Aliquot of 10 μl cell lysate containing 1 mg total protein was added to each lane. *c,* cell lysates (100 μl) from control, T4-60 cells, and cells expressing Trp3 (T3) or C-terminal HA-tagged Trp4 [T4(HAc)] were immunoprecipitated with the anti-NHERF, IC270. The precipitates were separated by 8% SDS-PAGE and then probed with the anti-Trp4 C-terminal, T4cAb (left) or the anti-Trp4 N-terminal, T4nAb (right), to reveal coprecipitation of Trp4 with NHERF. *d,* cell lysates (100 μl) were immunoprecipitated with anti-Trp4 N-terminal antibody and the presence of the HA-tagged Trp4 was determined by immunoblotting using the anti-HA monoclonal antibody, 12CA5. Molecular weights as revealed by prestained protein markers are indicated to the left.

Figure 4. Coassembly of PLCβ1, Trp4 and NHERF in T4-60 cells. *a,* detection of PLCβ1 in control (C) and T4-60 (T4) cells by immunoblotting using the anti-PLCβ1 antibody. A 100 kD

and a 150 kD forms are commonly detected in cell lines and freshly isolated tissues by this antibody and probably represent alternatively spliced forms of PLCβ1 or proteolytic degradation during sample processing (*37*). The higher molecular weight bands are common for the HEK cells as they were also seen by others using the same antibody (*37*). Aliquot of 10 μl total cell lysate was used in each lane. *b*, PLCβ1 immunocoprecipitated with NHERF and Trp4. T4-60 cell lyaste (100 μl) in RIPA buffer was subjected to immunoprecipitation by the anti-NHERF, IC270 or the anti-Trp4, T4cAb. The precipitates were separated by 8% SDS-PAGE, transferred to nitrocellulose membrane, and probed with the anti-PLCβ1 antibody.

Figure 5. Coassembly of PLCβ1, Trp4 and NHERF in mouse brain. *a*, expression of PLCβ1 (left), NHERF (middle) and Trp4 (right) in mouse brain. A whole brain from an adult mouse was homogenized in 1 ml RIPA buffer as described in the Experimental Procedures. Aliquot of 10 μl (1.4 mg total protein) lysate was subjected to 8% (for PLC) or 10% (for NHERF) SDS-PAGE. Proteins were transferred and probed with antibodies against PLCβ1 or NHERF. Under the same conditions, the anti-Trp4 antibody failed to detect any signal at the expected size range. Therefore, 200 μl whole brain lysate was immunoprecipitated with the anti-Trp4, T4cAb, and the precipitates were separated by 8% SDS-PAGE, transferred, and then probed again with T4cAb. Arrowheads indicate the two bands corresponding to the sizes of Trp4α and Trp4β. The identities for the higher molecular weight bands are not known as they appeared in some but not all blots. *b*, association of Trp4 with NHERF in brain. Brain lysate (200 μl) was immunoprecipitated with antibodies against HisTag, NHERF, or Trp4. The presence of Trp4 in the immunoprecipitates was examined by immunoblotting using the anti-Trp4, T4cAb. Anti-HisTag was used as a negative control for immunoprecipitation. *c*, PLCβ1

immunocoprecipitated with Trp4 and NHERF from brain. Brain lysate was immunoprecipitated with antibodies against HisTag, NHERF, or Trp4. The presence of PLCβ1 in the immunoprecipitates was examined by immunoblotting using the anti-PLCβ1 antibody.

Fig. 1

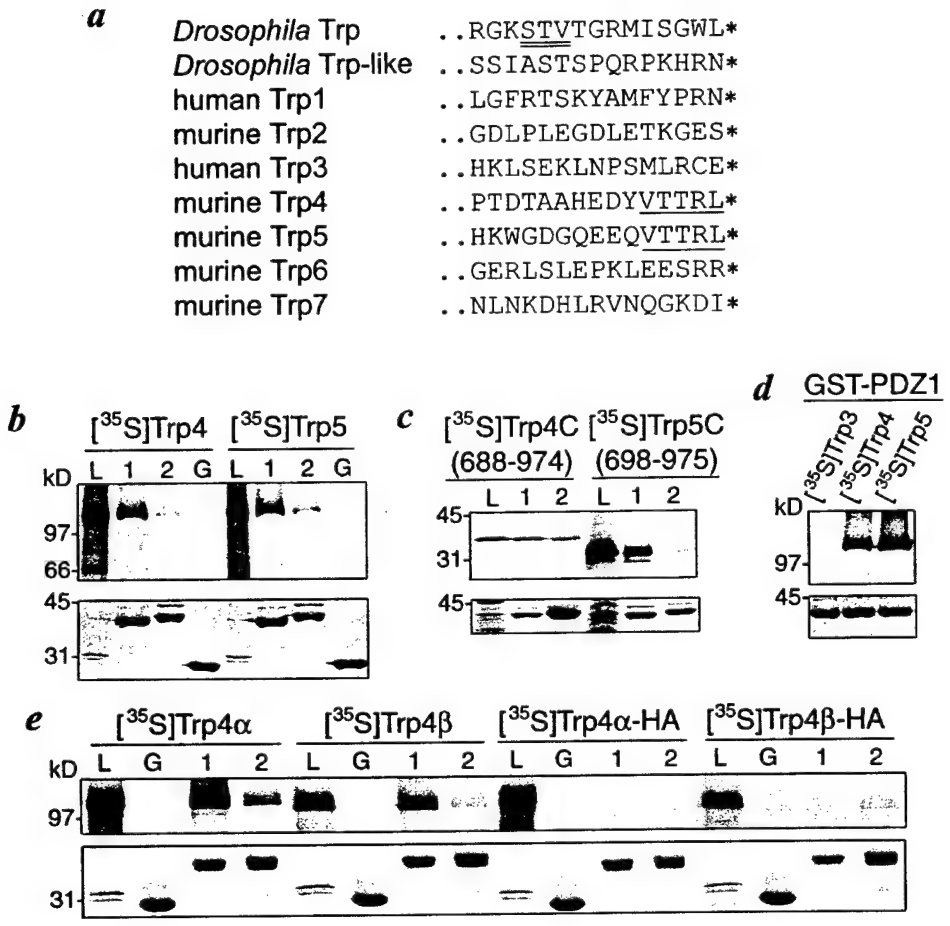
a
Drosophila Trp ..RGKSTVTGRMISGWL*
Drosophila Trp-like ..SSIASTSPQRPKHRN*
human Trp1 ..LGFRTSKYAMFYPRN*
murine Trp2 ..GDLPLEGDLETKGES*
human Trp3 ..HKLSEKLNPSMLRCE*
murine Trp4 ..PTDTAAHEDYVTTRL*
murine Trp5 ..HKWGDGQEEQVTTRL*
murine Trp6 ..GERLSLEPKLEESRR*
murine Trp7 ..NLNKDHLRVNQGKDI*
b
[35S]Trp4
[35S]Trp5
kD
L 1 2 G L 1 2 G
97
66
45
31
c
[35S]Trp4C (688-974)
[35S]Trp5C (698-975)
L 1 2 L 1 2
45
31
45
d
GST-PDZ1
[35S]Trp3
[35S]Trp4
[35S]Trp5
kD
97
45
e
[35S]Trp4α
[35S]Trp4β
[35S]Trp4α-HA
[35S]Trp4β-HA
kD
L G 1 2 L G 1 2 L G 1 2 L G 1 2
97
31

Fig. 2

a

bovine PLCβ1 ..ELEGENPGKEFDTPL*
bovine PLCβ2 ..QDPLIAKADAQESRL*

b

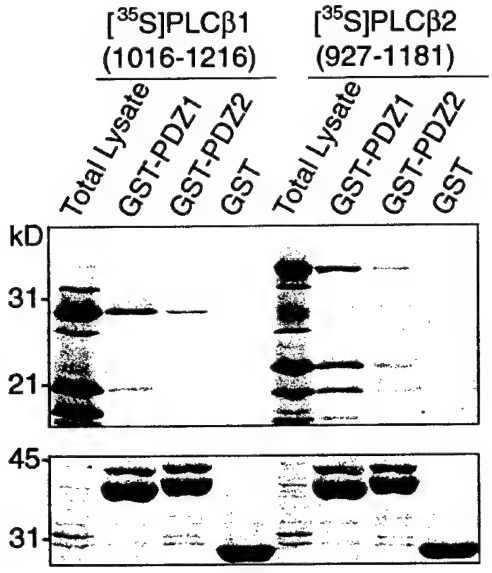

Fig. 3

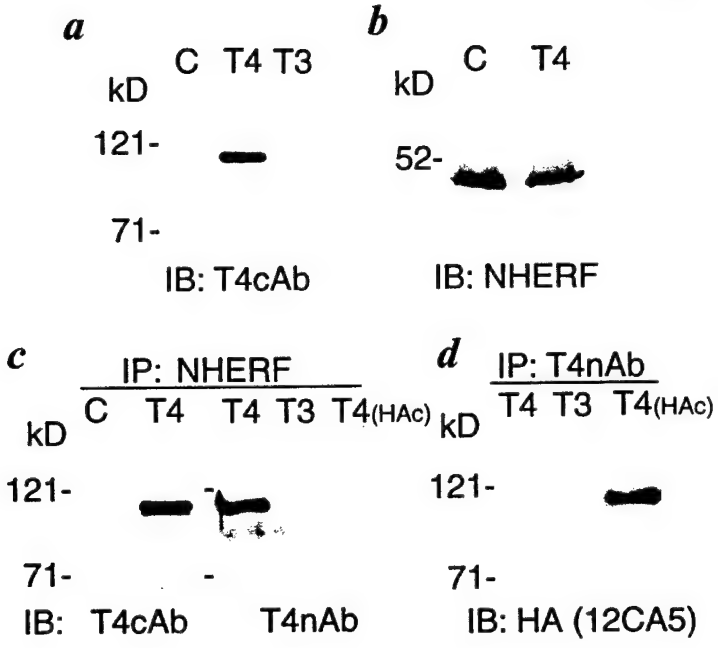
a
C T4 T3
kD
121-
71-
IB: T4cAb
b
C T4
kD
52-
IB: NHERF
c
IP: NHERF
C T4 T4 T3 T4(HAc)
kD
121-
71-
IB: T4cAb T4nAb
d
IP: T4nAb
T4 T3 T4(HAc)
kD
121-
71-
IB: HA (12CA5)

Fig. 4

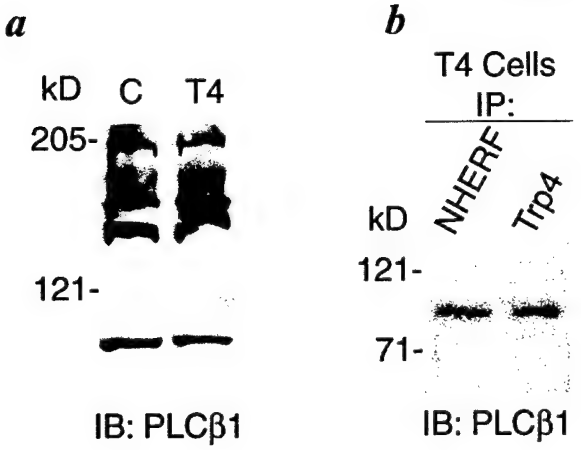
a
kD
C
T4
205-
121-
IB: PLCβ1
b
T4 Cells
IP:
NHERF
Trp4
kD
121-
71-
IB: PLCβ1

Fig. 5

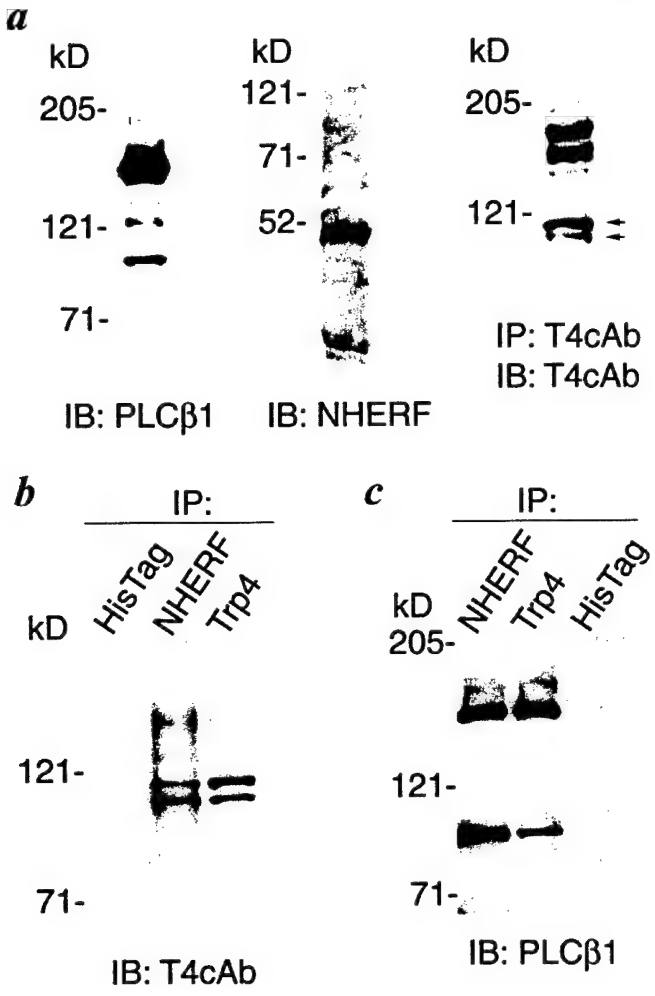
a
kD
205-
121-
71-
IB: PLCβ1
kD
121-
71-
52-
IB: NHERF
kD
205-
121-
IP: T4cAb
IB: T4cAb
b
IP:
HisTag
NHERF
Trp4
kD
121-
71-
IB: T4cAb
c
IP:
NHERF
Trp4
HisTag
kD
205-
121-
71-
IB: PLCβ1

NHE-RF, a merlin-interacting protein, is primarily expressed in luminal epithelia, proliferative endometrium and estrogen receptor-positive breast carcinomas

Anat O. Stemmer-Rachamimov*, Thorsten Wiederhold†, G. Petur Nielsen*, Marianne James†, Denise Pinney-Michalowski†, Jennifer E. Roy*, Wendy A. Cohen*, Vijaya Ramesh† and David N. Louis*

from the Molecular Neuro-Oncology Laboratory* and Molecular Neurogenetics Unit†, Departments of Pathology, Neurosurgery, Neurology and Genetics, Massachusetts General Hospital and Harvard Medical School, Boston, Massachusetts

Address correspondence to either Dr. David N. Louis, Molecular Neuro-Oncology Laboratory, CNY6, Massachusetts General Hospital, 149 Thirteenth St., Charlestown, MA 02129, 617-726-5510; 617-726-5079 (fax); email: louis@helix.mgh.harvard.edu or Dr. Vijaya Ramesh, Molecular Neurogenetics Unit, CNY6, Massachusetts General Hospital, 149 Thirteenth St., Charlestown, MA 02129, 617-724-9733; 617-726-3655 (fax) email: ramesh@helix.mgh.harvard.edu

Abstract

NHE-RF, a regulatory cofactor for NHE (Na+-H+ exchanger) type 3, interacts with ion transporters and receptors through its PDZ domains and with the MERM proteins (merlin, ezrin, radixin and moesin) via its carboxy terminus. Thus, NHE-RF may act as a multifunctional adaptor protein and play a role in the assembly of signal transduction complexes, linking ion channels and receptors to the actin cytoskeleton. NHE-RF expression is upregulated in response to estrogen in estrogen receptor (ER)-positive breast carcinoma cell lines, suggesting that it may be involved in estrogen signaling. To further understand NHE-RF function and its possible role in estrogen signaling, we analyzed NHE-RF expression in normal human tissues, including cycling endometrium, and in breast carcinomas, tissues in which estrogen plays an important role in regulating cell growth and proliferation. NHE-RF is expressed in many epithelia, especially in cells specialized in ion transport or absorption, and is often localized to apical (luminal) membranes. NHE-RF expression varies markedly in proliferative versus secretory endometrium, with high expression in proliferative (estrogen-stimulated) endometrium. Furthermore, ER status and NHE-RF expression correlate closely in breast carcinoma specimens. These findings support a role for NHE-RF in estrogen signaling.

Introduction

NHE-RF (Na+-H+ exchanger regulatory factor), a cytoplasmic phosphoprotein, was originally identified in the rabbit renal brush border as a co-factor required for cAMP/protein kinase A-mediated inhibition of NHE (Na+-H+ exchanger) type 3.[1] The human homologue was identified from human placenta and has also been referred to as EBP50 (ezrin binding protein).[2] NHE-RF is a 358 amino-acid protein with two homologous PDZ domains, which mediate protein-protein interactions. A related protein, NHE-RF2 (also known as E3KARP), was isolated from small intestine and renal brush border and shares 51% identity with NHE-RF, primarily in the PDZ domains.[3] PDZ-containing proteins are often localized at the plasma membrane and appear to promote the assembly of membrane-bound macromolecular complexes (transduction complexes), into which target molecules are recruited. Many PDZ domains-containing-proteins are involved in cell signaling.[4-6]

NHE-RF interacts, via its PDZ domains, with a variety of ion transport proteins such as the cystic fibrosis transmembrane regulator, the sodium-bicarbonate co-transporter, as well as with membrane receptors such as the β2 adrenergic and the purinergic P2Y1. Recently, we and others have shown that NHE-RF directly interacts with merlin, the *NF2* (neurofibromatosis 2)-encoded tumor suppressor protein, and with ezrin, radixin and moesin (MERM proteins), which are involved in cytoskeletal reorganization and signal transduction.[7] The MERM binding region is a non-PDZ site in the C-terminus.[8] Thus, NHE-RF may also be involved in the assembly of transduction complexes that link membrane receptors and transporters with intracellular signaling components.

Interestingly, NHE-RF expression is upregulated in response to estrogen in estrogen receptor (ER)-positive breast carcinoma cell lines (reference 9 and Ramesh, unpublished data). NHE-RF expression in these cells is mediated by the estrogen receptor

and suppressed by antiestrogens.[9] These findings suggest a role for NHE-RF in the estrogen signal transduction cascade in estrogen-responsive tissues. To gain more insight into the physiological relevance of NHE-RF, we performed a comprehensive expression study of the protein in normal adult human tissues. In order to evaluate the relationship between estrogen and NHE-RF expression in normal and malignant estrogen-responsive tissues, we also examined NHE-RF expression in cycling endometrium, as well as in ER-positive and ER-negative breast carcinomas.

Materials and Methods

Tissues. Formalin-fixed, paraffin-embedded sections of normal adult human organs from surgical specimens and autopsies were obtained from the Department of Pathology at Massachusetts General Hospital. We examined two to five samples from each paraffin-embedded organ. Organs examined included: brain and spinal cord, peripheral nerve, pituitary gland, placenta, kidney, skin, muscle, endometrium, breast, esophagus, stomach, small and large intestines, liver, spleen, pancreas, salivary glands, thyroid, tonsils, heart and lungs. To evaluate the possible association between estrogen and NHE-RF expression in normal tissues, we examined multiple samples of proliferative and secretory endometrium. To assess the possible association between estrogen receptor status and NHE-RF expression in breast carcinomas, we studied eighteen invasive breast carcinomas for which estrogen receptor status has been previously determined by immunohistochemistry.

Cell lines. Breast cancer cell lines, MCF-7, ZR-75-B, T-47D, MCF-7-ADR and MDA-MB-231, were obtained from the Massachusetts General Hospital Cancer Center and normal breast epithelial cell lines, HBL-100, MCF-12-F, were obtained from ATCC. Cell lines were maintained in DMEM with 10% fetal calf serum.

Antibodies. The polyclonal IC270 antibody is directed at the GST-NHE-RF fusion protein and has been characterized elsewhere.[10,11] A commercial antibody (Estrogen Receptor, Clone 1D5, DAKO, Carpinteria, CA) was used to evaluate estrogen receptor status; this antibody recognizes both the α and β forms of the receptor.

Western blot analysis. Protein lysates were prepared from cells in phosphate buffered saline (PBS) containing 2% sodium dodecyl sulfate (SDS) and a cocktail of protease inhibitors (Boehringer Mannheim, Indianapolis, In). Protein concentrations were measured using the DC protein assay system (Bio-Rad, Melville, NY). Three hundred μg of total cellular protein were subjected to SDS-polyacrylamide gel electrophoresis and transferred to nitrocellulose membranes (Bio-Rad, Melville, NY). Blots were then probed with the NHE-RF antibody IC270 (affinity eluted 1:50. Proteins were visualized with anti-rabbit horseradish peroxidase-conjugated secondary antibody and the ECL chemiluminescence system (Amersham Inc, Arlington Heights, Il). Signal intensity was quantified by densitometric scanning of autoradiographs using transmittance analysis (Fluor-S, Multiimager, Bio-Rad, Melville, NY).

Immunohistochemistry. Immunohistochemistry for NHE-RF was perfomed using IC270. Formalin-fixed, paraffin-embedded, eight-micron-thick sections were deparaffinized, rehydrated, immersed in 0.5% H_2O_2/methanol for 20 minutes and rehydrated in graded ethanols. For antigen retrieval, sections were microwaved in 0.01M sodium citrate buffer (pH 6.0) for 15 minutes. Sections were then blocked in 10% normal goat serum and 5% milk in 1% bovine serum albumin (BSA) in PBS, followed by incubation with primary antibody overnight at 4°C. Incubation with biotinylated goat anti-rabbit antibody (Vector Laboratories, Burlingame, CA) for 30 minutes at room temperature was followed by the standard avidin-biotin-complex (ABC) process (Vectastain Elite ABC kit, Vector Laboratories, Burlingame, CA). Diaminobenzidine (DAB) was used as a chromogen, followed by counterstaining with hematoxylin. Positive controls included paraffin-embedded human placenta sections as well as formalin fixed, paraffin-embedded cell pellets from MCF-7 and MCF-7-ADR cell lines, which express high levels or low levels of NHE-RF, respectively, as shown in Western blot analysis (see below). For negative controls, the primary antibody was omitted and prior immunostaining with preabsorbed serum did not

reveal any specific reactivity.[12] To control for possible effects of fixation and antigen retrieval, frozen sections of human placenta were also immunostained. Immunohistochemistry for estrogen receptors (ER) was performed according to standard procedures. Briefly, antigen retrieval was achieved by microwaving the sections in Tris buffer (pH 10) for 10 min. Sections were blocked with 10% normal horse serum and incubated with ER antibodies (1:100 dilution) overnight at 4°C. Sections were incubated with secondary antibodies at room temperature for 45 minutes followed by the ABC reaction, visualization with DAB and counterstaining with hematoxylin.

Results

Western blotting and immunohistochemistry for NHE-RF in cell lines

Quantitative Western blot analysis, performed three times, confirmed that three estrogen receptor-positive breast cancer cell lines, MCF-7, ZR-75-B, and T-47D, had 9.50 ± 2.20-fold higher levels of NHE-RF when compared to the normal mammary lines HBL-100 and MCF-12-F (Figure 1). Expression of NHE-RF was expressed at only low levels in the estrogen receptor-negative breast cancer lines MCF-7-ADR and MDA-MB-231 and was not detectable in the breast cancer cell line DU4475. Immunocytotochemical staining of cell pellets from MCF-7 and MCF-7-ADR with the IC270 antibody showed strong expression only in MCF-7, the ER-positive cell line (Figure 2A).

Immunohistochemistry for NHE-RF expression in normal adult tissues

NHE-RF is expressed in many tissues but has a highly selective cellular and subcellular distribution. Intense NHE-RF expression was seen in epithelial cells of many organ systems, especially in cells that perform an absorptive function, possess microvilli, or are involved in ion transport. Immunohistochemistry of paraffin-embedded sections of placenta demonstrated a characteristic pattern of NHE-RF expression, with prominent expression in the syncytiotrophoblast, the outer cell layer of placental villi, and its brush border, whereas the villous mesenchyme was immunonegative. Frozen sections of placenta showed the same pattern of immunostaining. All negative controls showed no staining.

As previously demonstrated using immunofluorescence,[12] strong expression of NHE-RF was seen in the renal proximal tubules with prominent staining of the luminal cell membrane and the microvillous brush border (Figure 2B). The parietal epithelium lining Bowman's capsule of the renal glomeruli also showed prominent positivity, while the mesangium and glomerular endothelium were immunonegative and the distal tubules and collecting tubules had only weak cytoplasmic staining.

A highly selective pattern of expression of NHE-RF was also seen in the gastro-intestinal system. In the stomach, fundic glands showed strong expression in parietal cells, whereas chief cells, mucin-secreting cells and surface epithelium were immunonegative. In the small bowel, the protein is abundant at the apical surface of absorptive cells and in microvilli extending from the cell surface, but is absent in intercalated goblet cells. Similarly, in the large bowel, absorptive cells of the surface epithelium and colonic crypts show strong membranous staining of the luminal border, but adjacent intercalated goblet cells were immunonegative (Figure 2C).

Stratified squamous epithelium in the esophagus, skin, and tonsils showed only weak to moderate cytoplasmic staining, more pronounced in the deep layers. Eccrine glands in the skin, however, showed cytoplasmic immunostaining with strong apical membranous expression, highlighting intercalated canaliculi. In contrast, the underlying myoepithelial cells were immunonegative. Other skin adenexa, such as the pilar unit, showed weak diffuse cytoplasmic staining. In the salivary glands, NHE-RF was weakly expressed in the cytoplasm of serous acinar cells, but there was prominent linear luminal membranous immunostaining. The mucinous acinar cells of the salivary glands were immunonegative. Similarly, acinar cells of the pancreas showed weak cytoplasmic staining and luminal linear immunopositivity, while cells of the islands of Langerhans were immunonegative. In the anterior pituitary, selected cells were moderately immunopositive. The posterior pituitary was immunonegative, as was the thyroid gland. In the breast, ductal and acinar epithelia were immunopositive, with apical membranous staining of the acinar epithelial cells (Figure 2D).

Skeletal muscle and myocardium were immunonegative for NHE-RF, while smooth muscle, particularly vascular smooth muscle, showed moderate immunopositivity in most tissues. In the lung, bronchial epithelium was only weakly positive and alveolar pneumocytes were immunonegative. In the liver, hepatocytes and Kupffer cells showed no expression of NHE-RF and only weak to moderate expression was seen in ductal

epithelium. Focal, moderate positivity was seen in the white pulp of the spleen and in scattered lymphocytes in germinal centers of lymph nodes.

In the brain and spinal cord, neurons and resting glia did not express NHE-RF. Strong expression of NHE-RF, however, was observed in glial process in areas of chronic reactive gliosis, such as subpial region, or in proliferating Bergmann glia in the cerebellum. Marked NHE-RF expression was also observed at the apical membranes of ependymal cells. Interestingly, this pattern of expression was altered in buried ependymal cells found just below the ventricular surface, in which NHE-RF was seen as an area of strong cytoplasmic immunopositivity without polarized apical or membranous staining. Arachnoid cells were immunonegative, as were Schwann cells in peripheral nerves.

Immunohistochemistry for NHE-RF expression in endometrium

Proliferative endometrium showed strong expression of NHE-RF in the cytoplasm and luminal membrane of glandular epithelium as well as in scattered stromal cells (Figure 2F). NHE-RF was expressed in essentially all epithelial cells in the proliferative endometrium samples. In contrast, there was only weak expression of NHE-RF in the glandular epithelium of secretory endometrium and adjacent stroma (Figure 2E).

Immunohistochemistry for NHE-RF expression in primary breast tumors

Examination of sections from 18 infiltrating breast adenocarcinomas showed strong correlation between positive immunostaining for ER and high expression of the NHE-RF protein: ten of 11 (> 90%) of the ER-positive tumors strongly expressed NHE-RF. On the contrary, five of seven ER-negative tumors did not express NHE-RF (Figures 2G-H, Table 1). In those tumors that were NHE-RF immunopositive, staining was observed in nearly all tumor cells, contrasting with the adjacent immunonegative stroma. NHE-RF positivity was present as membranous staining, especially at the luminal aspects of cells, and as diffuse cytoplasmic staining.

Discussion

NHE-RF is highly expressed in epithelia of many tissues, particularly in cells with numerous microvilli, and is often concentrated at the luminal membrane. Prominent NHE-RF expression is seen in cells specialized in ion transport: renal proximal tubules, eccrine glands, colonic absorptive cells, parietal cells in gastric glands and ependymal cells. These findings support the proposed role of NHE-RF as a regulator of membrane protein transporters, and confirm Northern blot data showing high NHE-RF mRNA levels in human tissues containing polarized epithelia such as the mammary gland, kidney, small intestines and salivary gland.[9]

The association between estrogen stimulation and NHE-RF expression in normal endometrium and in breast carcinomas suggests that NHE-RF must be a multifunctional protein, with additional roles to those of ion transport. Specific and early induction of NHE-RF mRNA by estrogen has been observed in breast carcinoma cells.[9] The present observations extend the correlation between ER status and NHE-RF expression in breast cancer to primary human tumors, and raise the possibility that NHE-RF may play a role in estrogen-mediated cell growth. The proliferative effects of the estrogen are mediated through ER, an intracellular nuclear receptor that, when bound to estrogen, is transformed into an active transcription factor and regulates the expression of a variety of genes. Antiestrogens may therefore be therapeutically effective in ER-positive breast cancers. ER-negative tumors, however, are more aggressive tumors, associated with early recurrence and poor patient survival, and do not generally respond to antiestrogen treatment. However, about 40% of patients with ER-positive cancer do not respond to endocrine manipulations, and about 10% of ER-negative tumors respond.[13,14] The factors that lead to the conversion of an ER-positive, responsive breast cancer into a hormone-refractory tumor are poorly understood, and encourage further study of mechanisms of ER-mediated cell growth.

Estrogens induce cytoskeletal changes in ER-positive breast cancer cells that include an increase in the number and size of microvilli,[15,16] as well as increased expression of cytokeratins associated with the nuclear matrix-intermediate filament system.[17] Interestingly, alterations of the nuclear matrix-intermediate filament system, an extensive network that connects the plasma membrane and cytoskeleton with the nuclear membrane and nuclear matrix, can mediate changes in gene expression.[18,19] NHE-RF, an early response gene to estrogen stimulation, may therefore play a role in the assembly of an estrogen transduction complex by linking the actin cytoskeleton to an anchored membrane protein. NHE-RF could bind a transduction complex via interaction with MERM proteins at a C-terminal, non-PDZ site, and to a membrane protein via one of the PDZ domains. NHE-RF may also be involved in cross-talk among signal transduction pathways. Several signaling cascades, including epidermal growth factor and tyrosine kinase/MAP-kinase pathways, are involved in estrogen signaling;[20-23] such overlapping pathways may partly explain how breast cancer cells adapt to and bypass estrogen receptors blocked by antiestrogen therapy. It is possible that an alternative pathway for estrogen signaling in ER-negative breast carcinomas might involve NHE-RF expression, via ER-independent upregulation, which could explain the 30% of ER-negative tumors expressing NHE-RF in our series.

These studies suggest that NHE-RF acts as a multifunctional protein, has potential roles in the apical surfaces of ion transporting epithelium as well as in estrogen-mediated growth control. The data encourage further study of NHE-RF in breast carcinomas to increase understanding of the growth control mechanisms in these hormonally-regulated tumors, and to develop novel means to interfere therapeutically in such growth pathways.

Acknowledgments

This work was supported by NIH NS24279 and a U.S. Army grant. T.W. was supported by a Gottlieb Daimler and Karl Benz predoctoral fellowship.

References

1. Weinman EJ, Steplock D, Wang Y, Shenolikar S: Characterization of a protein cofactor that mediates protein kinase A regulation of the renal brush border membrane Na(+)-H+ exchanger. J Clin Invest 1995, 95:2143-9
2. Reczek D, Berryman M, Bretscher A: Identification of EBP50: A PDZ-containing phosphoprotein that associates with members of the ezrin-radixin-moesin family. J Cell Biol 1997, 139:169-79
3. Yun CH, Oh S, Zizak M, Steplock D, Tsao S, Tse CM, Weinman EJ, Donowitz M: cAMP-mediated inhibition of the epithelial brush border Na+/H+ exchanger, NHE3, requires an associated regulatory protein [published erratum appears in Proc Natl Acad Sci U S A 1997 Sep 2;94(18):10006]. Proc Natl Acad Sci U S A 1997, 94:3010-5
4. Doyle DA, Lee A, Lewis J, Kim E, Sheng M, MacKinnon R: Crystal structures of a complexed and peptide-free membrane protein- binding domain: molecular basis of peptide recognition by PDZ. Cell 1996, 85:1067-76
5. Morais Cabral JH, Petosa C, Sutcliffe MJ, Raza S, Byron O, Poy F, Marfatia SM, Chishti AH, Liddington RC: Crystal structure of a PDZ domain. Nature 1996, 382:649-52
6. Fanning AS, Anderson JM: Protein-protein interactions: PDZ domain networks. Curr Biol 1996, 6:1385-8
7. Murthy A, Gonzalez-Agosti C, Cordero E, Pinney D, Candia C, Solomon F, Gusella J, Ramesh V: NHE-RF, a regulatory cofactor for Na(+)-H+ exchange, is a common interactor for merlin and ERM (MERM) proteins. J Biol Chem 1998, 273:1273-6
8. Reczek D, Bretscher A: The carboxyl-terminal region of EBP50 binds to a site in the amino- terminal domain of ezrin that is masked in the dormant molecule. J Biol Chem 1998, 273:18452-8

9. Ediger TR, Kraus WL, Weinman EJ, Katzenellenbogen BS: Estrogen receptor regulation of the Na+/H+ exchange regulatory factor. Endocrinology 1999, 140:2976-82

10. Gonzalez-Agosti C, Wiederhold T, Herndon ME, Gusella J, Ramesh V: Interdomain interaction of merlin isoforms and its influence on intermolecular binding to NHE-RF. J Biol Chem 1999, 274:34438-42

11. Gonzalez-Agosti C, Xu L, Pinney D, Beauchamp R, Hobbs W, Gusella J, Ramesh V: The merlin tumor suppressor localizes preferentially in membrane ruffles. Oncogene 1996, 13:1239-1247

12. Breton S, Wiederhold T, Marshansky V, Nsumu NN, Ramesh V, Brown D: The B1 subunit of the H+ATPase is a PDZ-domain binding protein: Colocalization with NHE-RF in renal B-intercalated cells. J Biol Chem 2000, 275:18219-24

13. Nagai R, Kataoka M, Kobayashi S, Ishihara K, Tobioka N, Nakashima K, Naruse M, Saito K, Sakuma S: Estrogen and progesterone receptors in human breast cancer with concomitant assay of plasma 17beta-estradiol, progesterone, and prolactin levels. Cancer Res 1979, 39:1834-40

14. Henderson BE, Bernstein L, Ross R. Etiology of Cancer: Hormonal Factors. Cancer: Principles and Practice of Oncology. Ed. Fifth edition. Philadelphia:Lippincott-Raven, 1997.

15. Vic P, Vignon F, Derocq D, Rochefort H: Effect of estradiol on the ultrastructure of the MCF7 human breast cancer cells in culture. Cancer Res 1982, 42:667-73

16. Antakly T, Pelletier G, Zeytinoglu F, Labrie F: Changes of cell morphology and prolactin secretion induced by 2-Br- alpha-ergocryptine, estradiol, and thyrotropin-releasing hormone in rat anterior pituitary cells in culture. J Cell Biol 1980, 86:377-87

17. Coutts AS, Davie JR, Dotzlaw H, Murphy LC: Estrogen regulation of nuclear matrix-intermediate filament proteins in human breast cancer cells. J Cell Biochem 1996, 63:174-84

18. Blum JL, Wicha MS: Role of the cytoskeleton in laminin induced mammary gene expression. J Cell Physiol 1988, 135:13-22

19. Seely KA, Aggeler J: Modulation of milk protein synthesis through alteration of the cytoskeleton in mouse mammary epithelial cells cultured on a reconstituted basement membrane. J Cell Physiol 1991, 146:117-30

20. Katzenellenbogen BS: Estrogen receptors: bioactivities and interactions with cell signaling pathways. Biol Reprod 1996, 54:287-93

21. Smith CL: Cross-talk between peptide growth factor and estrogen receptor signaling pathways. Biol Reprod 1998, 58:627-32

22. Aronica SM, Katzenellenbogen BS: Stimulation of estrogen receptor-mediated transcription and alteration in the phosphorylation state of the rat uterine estrogen receptor by estrogen, cyclic adenosine monophosphate, and insulin-like growth factor-I. Mol Endocrinol 1993, 7:743-52

23. Migliaccio A, Pagano M, Auricchio F: Immediate and transient stimulation of protein tyrosine phosphorylation by estradiol in MCF-7 cells. Oncogene 1993, 8:2183-91

Figure legends

Figure 1. Western blot analysis, using affinity eluted IC270 antibody at 1:50 dilution, of mammary epithelial and breast cancer cell lines showing high NHE-RF expression in the ER-positive cell lines, T-47D, ZR-75-B and MCF-7. The arrow indicates NHE-RF at 50 kDa.

Figure 2. NHE-RF expression in normal and neoplastic tissues, immunostained with IC270 antibody. **(A)** NHE-RF expression in breast carcinoma cell lines: low expression in estrogen receptor (ER) negative MCF-7-ADR (left); strong expression in ER positive MCF-7 cells (right). **(B-F)** NHE-RF expression in normal tissues: **(B)** Strong membranous expression of NHE-RF in proximal tubular epithelium and parietal epithelial cells of Bowman's capsule. **(C)** NHE-RF expression in apical surface of absorptive cells in colonic glands; goblet cells are immunonegative. **(D)** Strong expression of NHE-RF in luminal membrane of ducts and acini in the breast. **(E)** Low NHE-RF expression in secretory endometrium, **(F)** High expression of NHE-RF in proliferative endometrium. **(G-H)**. Expression of NHE-RF in breast carcinomas. **(G)** High expression of NHE-RF in ER-positive breast carcinoma. **(H)** ER-negative breast carcinoma immunonegative for NHE-RF.

Table 1. NHE-RF and ER expression in 18 primary breast carcinomas. NHE-RF immunostaining intensity: (-) = none or minimal, (++) = moderate, (+++) = intense positivity. When positive, nearly all cells are positive.

FIGURE 1

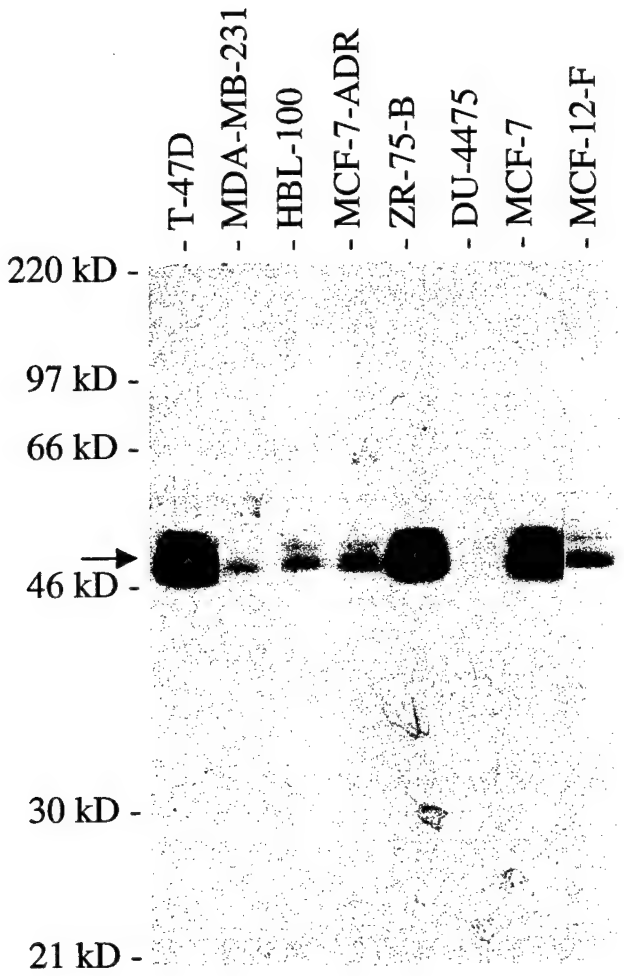
T-47D
MDA-MB-231
HBL-100
MCF-7-ADR
ZR-75-B
DU-4475
MCF-7
MCF-12-F
220 kD
97 kD
66 kD
46 kD
30 kD
21 kD

FIGURE 2

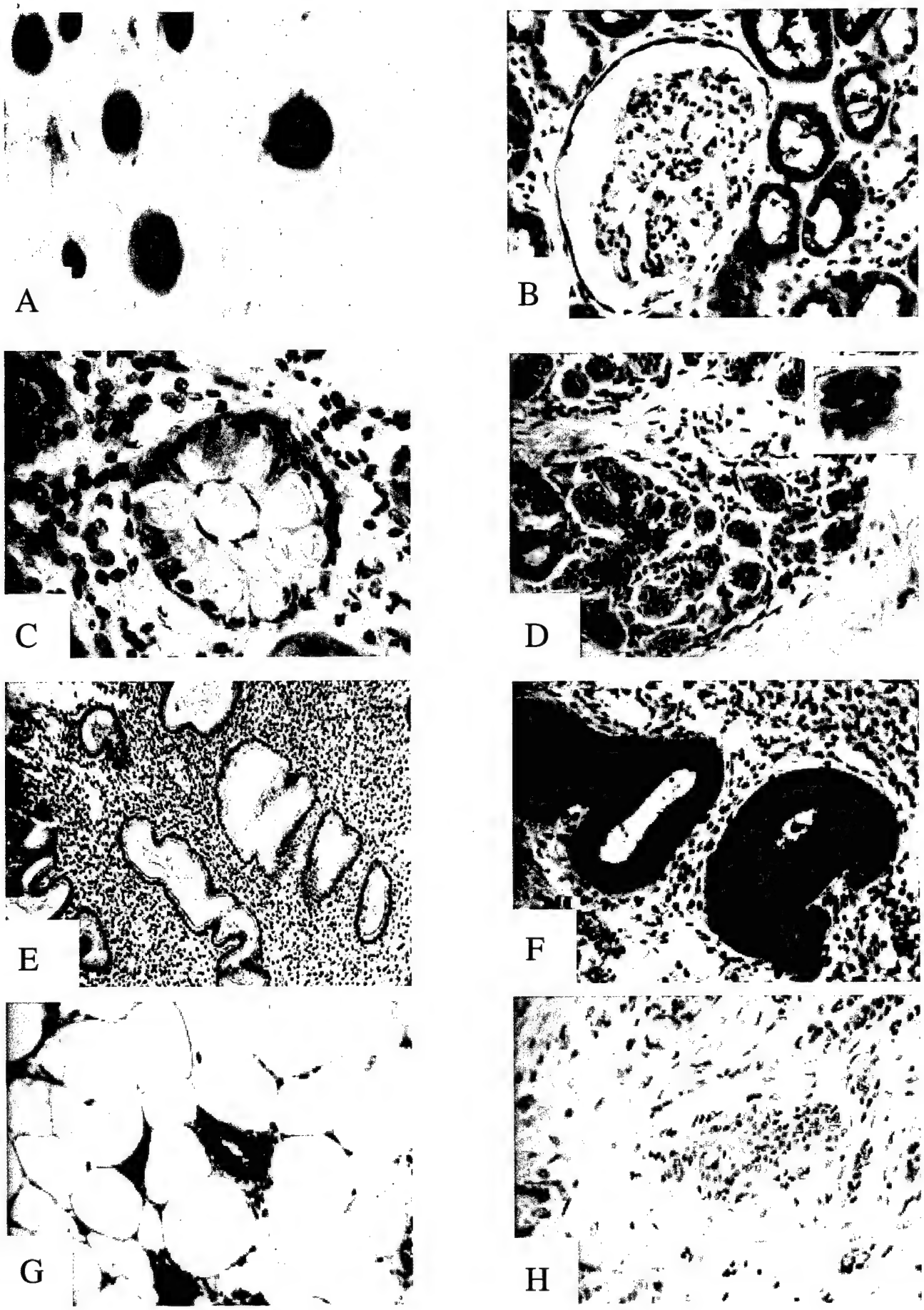

Table 1.

Tumor Sample	NHE-RF IHC	ER status
BC1	+++	POSITIVE
BC3	+++	POSITIVE
BC5	+++	POSITIVE
BC9	+++	POSITIVE
BC10	+++	POSITIVE
BC11	+++	POSITIVE
BC4	++	POSITIVE
BC7	++	POSITIVE
BC12	++	POSITIVE
BC14	++	POSITIVE
BC8	-	POSITIVE
BC6	++	NEGATIVE
BC15	++	NEGATIVE
BC2	-	NEGATIVE
BC13	-	NEGATIVE
BC16	-	NEGATIVE
BC17	-	NEGATIVE
BC18	-	NEGATIVE

Merlin selectively binds F- but not G-actin, and stabilizes the filaments through a lateral association

Marianne F. James*, Nitasha Manchanda*, Charo Gonzalez-Agosti*†, John H. Hartwig‡ and Vijaya Ramesh*[1]

*Molecular Neurogenetics Unit, Massachusetts General Hospital, Charlestown, MA 02129, †Present address: Psychiatry Research, University of Zurich, Zurich, Switzerland. ‡Division of Experimental Medicine, Brigham and Women's Hospital, Harvard Medical School, Boston, MA 02215.

Running title: Merlin-Actin Interaction

Address correspondence to:

[1]Dr. Vijaya Ramesh

Bldg. 149, 13th Street

Charlestown, MA 02129

Ph: (617) 724 9733; Fax: (617) 726 3655

E-mail:ramesh@helix.mgh.harvard.edu

SYNOPSIS

The neurofibromatosis 2 (NF2) protein product merlin, named for its relatedness to the ezrin, radixin, and moesin, (ERM) family of proteins, is a tumor suppressor whose absence results in the occurrence of multiple nervous system tumors, particularly schwannomas and meningiomas. Merlin's similarity to ERMs suggests it may share functions, acting as a link between cytoskeletal components and the cell membrane. The N-terminus of merlin has strong sequence identity to the N-terminal actin-binding region of ezrin. Here, we describe in detail the merlin-actin interaction and show that recombinant merlin isoform 1 and 2 differentially bind actin filaments, suggesting that the intramolecular interactions in isoform 1 may hinder its ability to bind actin. Merlin isoform 2 binds F-actin with an apparent binding constant of 3.6 μM and a stoichiometry of 1 mole merlin per 11.5 moles of actin in filaments at saturation and does not bind G-actin. Merlin isoform 2 and the N-terminal domain, slow actin filament disassembly further demonstrating that merlin binds periodically along F-actin. This is further supported by electron microscopy data, which shows merlin to be bound to cytoskeletal actin filaments. Comparison of these findings to those reported for ERM proteins reveal a distinct role for merlin in actin filament dynamics.

Key words: Neurofibromatosis 2, merlin, actin cytoskeleton, ERM

INTRODUCTION

Merlin, the tumor suppressor protein deficient in neurofibromatosis 2 (NF2),[2] has high structural and sequence similarity to the ezrin, radixin, and moesin (ERM) family of cytoskeleton-plasma membrane linker proteins [1]. Merlin is 63% identical to the ERM proteins at the N-terminus, a region recently designated as the FERM (4.1 and ERM) domain [2]. In ERM proteins, the FERM domain binds directly to the cytoplasmic domains of several integral membrane proteins such as CD44, CD43, ICAM-1, -2, and -3 [3, 4]. In addition, these domains in merlin and ERM proteins (MERM) bind the C-termini of the cytoplasmic adaptor protein, Na^+-H^+ exchanger regulatory factor, NHE-RF [5, 6], and its related family member NHE-RF2 [7]. The interaction of NHE-RF and NHE-RF2, via their PDZ domains, with multiple ion channels and receptors, may potentially associate the MERM proteins to the Na^+/H^+ exchanger type 3, β_2-adrenergic receptor, purinergic P2Y1 receptor, cystic fibrosis transmembrane conductance regulator, the Na^+/HCO_3^- cotransporter and the vacuolar proton pump H^+-ATPase [7-13].

In MERM proteins, the FERM domain is followed by an extended α-helical region and a charged C-terminus, although merlin maintains only 21 and 35% sequence similarity to each region, respectively, with the ERM proteins [2]. Moreover, unlike the ERM proteins, merlin exists as two major isoforms distinguished by alternative C-termini. Merlin isoform 1 is a 595 amino acid protein, derived from 16 constitutive exons, 1-15 and 17, while isoform 2 is a 590 amino acid protein resulting from the alternatively-spliced exon 16, replacing 16 C-terminal amino acids with 11 novel residues [1]. The C-termini of both isoforms of merlin were shown to bind βII-spectrin, with isoform 2 binding more effectively [14].

In view of the multiple ligands identified for ERM proteins, it has been proposed that the ability to homo- and heterotypically associate with each other may regulate their activities [3, 4].

The intra- or intermolecular interaction of specific N- and C-ERM association domains (ERMADs) results in folded ("closed") and inactive ERM proteins due to the masking of their N- and C-terminal ligand binding sites [3, 4]. Merlin isoform 1, likewise is capable of these "head-to-tail" interactions, such that its N-terminus can associate with the C-termini of both isoform 1 as well as moesin, but not with the C-terminus of isoform 2. Therefore, merlin isoform 2 appears to exist in a constitutively "open" or active conformation due to its exposed ligand binding sites [15-18]. Phosphorylation and/or phosphatidylinositol 4,5-bisphosphate (PIP_2) binding appear to disrupt these intra- and intermolecular interactions, exposing the N- and C-terminal binding sites and, thereby, activating their respective plasma membrane-cytoskeletal cross-linking functions [4, 15, 19]

The C-termini of both ezrin and moesin bind directly to actin *in vitro* via a conserved actin-binding site contained in the last 34 amino acids [20-23]. Merlin lacks this domain owing to its partially divergent C-terminal sequence. Despite the lack of a conserved C-terminal actin binding domain, merlin localizes to actin-rich structures in cultured cells [24-27] and associates with the detergent-insoluble cytoskeletal fraction of cell lysates [26, 28, 29]. Recently, *in vitro* binding studies in ezrin revealed two additional actin binding sites at the N-terminus, aa 13-30 and aa 281-310, which bind F- and both F- and G-actin, respectively [30-32]. This actin binding region is highly conserved in merlin and the ability of merlin to bind actin through this domain was reported, although the influence of the interdomain self-association of merlin isoform 1 on actin binding was not addressed [33]. Another study did not observe this binding site in merlin isoform1 by ^{125}I-labeled F-actin blot overlays [18].

This study was undertaken to characterize in-depth merlin's association with actin, incorporating isoform specificity as well as quantitative and functional analyses. Using standard

cosedimentation and solid-phase binding assays we show that merlin's ability to self-interact in an isoform specific fashion alters its ability to bind actin and that the binding affinity for actin is distinct from that determined for ezrin. Pyrene-labeled actin disassembly assays provide evidence that merlin isoform 2 stabilizes actin filaments by binding to their sides and slowing actin disassembly. These results offer a more complete understanding of merlin's normal role as a cytoskeleton-associated membrane organizing protein which ultimately may aid in revealing how disruption of this function results in the loss of merlin's tumor suppressing capacity.

MATERIALS AND METHODS

Materials and antibodies

Actin isoforms were detected by Western blot analyses with a mouse monoclonal actin antibody (Sigma) and the glutathione-S-transferase (GST) protein was detected with monoclonal anti-GST (Santa Cruz Biotechnology). Merlin was detected using affinity-eluted rabbit polyclonal antibody N21 while electron microscopy implemented the mouse monoclonal antibody 1C4. These antibodies recognize both isoforms of merlin [24]. Purified actin was isolated from rabbit skeletal muscle (α-actin) and rabbit brain (β/γ-actin) as previously described [34]. All *in vitro* experiments were conducted using purified rabbit skeletal muscle α-actin unless otherwise specified. Monomeric pyrene-labeled rabbit skeletal muscle α-actin was prepared as described previously [34].

Preparation of recombinant merlin proteins

Human merlin full-length and truncated fusion proteins were expressed and purified from *Escherichia coli* [24]. Merlin deletion constructs with amino acids (aa) 1-332, 1-345, 340-595

and full-length isoform 1 (aa 1-595), and isoform 2 (aa 1-590) were expressed as glutathione S-transferase (GST) fusion proteins in pGEX2T. GST-fusion proteins were purified using Glutathione (GSH)-Sepharose 4B (Pharmacia) as previously described [24]. For assays where the GST moiety was removed, fusion proteins were treated with bovine thrombin (Sigma) for 2 h at room temperature.

Actin cosedimentation

All samples were precleared by centrifuging at 200,000 *g* (TLA 100 rotor; Beckman Instruments) for 20 min at 4°C. F-actin (α or β/γ), polymerized at 40 μM in Buffer B (10 mM HEPES, 100 mM KCl, 2 mM $MgCl_2$, 0.1 mM EGTA, 0.5 mM DTT, 0.5 mM ATP, pH 7.0)[34] for 30 min at 37 °C, was added to variable concentrations of merlin full-length or deletion constructs (0.05-3.0 μM) to a final concentration of 4 μM. Samples were incubated for 30 min at room temperature prior to centrifuging at 200,000 *g* for 20 min. Supernatant and pelleted samples were adjusted to 150 μl in SDS-PAGE sample buffer. Equal volumes of supernatant and pelleted samples, in the presence and absence of F-actin, were analyzed by 10% SDS-polyacrylamide gel electrophoresis (PAGE), and transferred electrophoretically to nitrocellulose membranes (Bio-Rad). The integrity of F-actin in pelleted samples was visualized using 0.2% Ponceau-S treated filters. Filters were immunoblotted with the N21 merlin antibody (1:100) and proteins were visualized using horseradish peroxidase (HRP)-conjugated secondary antibodies and the enhanced chemiluminescence (ECL) SuperSignal detection systems (Pierce). Assays were conducted in parallel in the absence of F-actin (self-pelleting) and standards for each concentration were run on separate gels in order to quantitate the value of total protein added (standard curves).

Quantitation of merlin-actin binding

The relative protein values used to determine the stoichiometry of merlin-to-actin binding were obtained from Western blots of sedimenting merlin, +/- actin, and known quantities of merlin, by scanning autoradiographs and immunoblots directly using the Flour-S Multiimager Analyzer (Biorad). The value of merlin full-length isoform 2 and N-terminal construct 1-332 binding to actin was obtained by calculating the difference between the values of pelleted merlin in the presence and absence of F-actin. These values were converted to molar concentrations based on the standard curve for each known merlin concentration. Actin saturation was determined by comparing the amount of merlin added to the amount of merlin bound. Linear transformation of these plots (Scatchard plot) provided a K_d and a stoichiometric molar ratio of merlin-to-actin binding. These data are representative of three independent sedimentation assays.

Solid-phase binding assays

GST-cleaved merlin isoforms 1 and 2, as well as N- and C-terminal deletion constructs, were assayed for F- and G-actin binding using a solid-phase protein-protein binding assay essentially as described [31]. Constant (2 μM) or titrated (0.5, 1, and 2 μM) recombinant merlin constructs or controls (BSA or GST) were coated in 96-well microtiter plates (Nunc) in 75 μl Buffer B (F-actin promoting buffer) at 37°C overnight. Wells were rinsed and residual-binding sites blocked in 2% BSA/coating buffer. After rinsing wells with the appropriate F- or G-actin buffer (Buffer A: 2 mM HEPES, 0.2 mM $MgCl_2$, 0.2 mM $CaCl_2$, 0.5 mM DTT, 0.5 mM ATP, pH 7.0), F- or G-actin (5 μM and 50nM, respectively) was added to each merlin-coated well for 1 h at room temperature. Wells were rinsed and protein complexes were eluted by adding 50 μl SDS-PAGE sample buffer to each well for 20 min at 65°C. Samples were resolved by SDS-PAGE,

transferred to nitrocellulose and immunoblotted using appropriate merlin or actin antibodies and detected using HRP-conjugated secondary antibodies and ECL detection systems (Amersham).

G-actin pull-down assays

GST pull-down assays were performed as described by Rohatghi et al., 1999 [35] with minor modifications. Equal amounts of GST-fusion proteins were immobilized on GSH-sepharose beads (Pharmacia) at a concentration of approximately 5 mg/ml packed beads. G-actin was thawed and precleared at 120,000 ***g*** to remove any polymerized actin. Approximately 5-10 μl of beads in 100 μl XB (10 mM HEPES, pH 7.6, 100 mM KCl, 1 mM $MgCl_2$, 0.1 mM EDTA, 1 mM DTT) plus 0.1% (v/v) Tween-20, 0.2 mM ATP, and 0.5 mg/ml ovalbumin, were incubated with 0.05 μM G-actin, a concentration below the barbed-end critical concentration. After gentle tumbling for 1 h at 4 °C, the beads were washed two times in 100 μl XB plus 0.1% (v/v) Tween-20 and 0.2 mM ATP. Proteins bound to the beads were eluted with SDS-PAGE sample buffer, resolved on a 10% Tris-HCl minigel (Bio-Rad) and immunoblotted with a monoclonal actin antibody. Purified NWIP (N-terminal WASP-interacting protein) was kindly provided by Dr. N. Ramesh of Children's Hospital, Boston, MA.

Fluorescent measurement of actin assembly/disassembly

The effect of full-length isoform 2 and N-terminal merlin 1-332 on the rate and extent of pyrene-labeled rabbit skeletal muscle actin was determined [34]. For actin polymerization assays, monomeric pyrene-labeled α-actin was polymerized to a final concentration of 1.5 μM in the presence or absence of either 0.03-1.5 μM GST-merlin isoform 2, N-terminal 1-332 or GST (control) proteins in Buffer B. For depolymerization assays, pyrene-labeled F-actin, at a

concentration of 10 μM, was diluted to 0.2 μM in the presence or absence of 0.004-0.2 μM merlin proteins in Buffer A [36]. The increase or decrease in the rate of fluorescence was monitored in a Perkin-Elmer model LS-50 fluorimeter using 366 and 386 nm as the excitation and emission wavelengths, respectively, over approximately 10 minutes. The final fluorescent readings for each sample were obtained at a single time point on the following day.

Electron microscopy

Immunogold labeling was conducted using the merlin monoclonal antibody, 1C4, on Triton X-100 permeabilized meningioma cells. Meningioma cells were plated on coverslips and permeabilized using PHEM-0.75% Triton X-100 buffer [34] containing 5 μM phallacidin and protease inhibitors for 2 min. Soluble proteins were removed using a PHEM buffer wash. Before labeling glass-adherent cytoskeletons with the anti-merlin IgG, residual fixative was blocked with 0.1% sodium borohydride in PHEM buffer and the coverslips containing the cytoskeletons were washed twice in PBS and twice in PBS containing 1% BSA, pH 8.2. Coverslips were covered with 25 μl of primary antibodies at a final concentration of 10μg/ml, incubated for 1 h at 25°C, and washed three times with PBS/BSA. Coverslips were then incubated for 1.5 h with a 1:20 dilution of goat anti-mouse IgG-coated 10 nm colloidal gold particles, washed three times in PBS/BSA and three times in PBS, and fixed with 1% glutaraldehyde in PHEM buffer for 10 min. Fixed specimens were washed extensively with distilled water, rapidly frozen, freeze-dried, and rotary-coated with 1.2 nm of tantalum-tungsten at 45° and 3.0 mm of carbon at 90° without rotation as previously described [37]. Cytoskeletons were examined and photographed in a JEOL 1200-EX electron microscope using a 100 kV accelerating voltage. No gold-labeling was found when primary IgG was omitted or when preimmune IgG was used as a control.

RESULTS

Cosedimentation of merlin with actin filaments

Using F-actin cosedimentation assays, we examined the ability of recombinant merlin isoforms as well as N- and C-terminal deletion constructs to bind F-actin. Variable concentrations of GST-merlin fusion proteins were incubated with a constant amount of polymerized F-actin, followed by high-speed centrifugation to pellet F-actin. Equal volumes of pelleted and supernatant material were solubilized in SDS-PAGE sample buffer and analyzed by Western blotting. Because ERM and merlin proteins characteristically aggregate and self-pellet [38], control assays were conducted in the absence of F-actin. Our results indicate that the merlin N-terminal segment, encompassing amino acids 1-332, and the alternatively-spliced full-length isoform 2, bind F-actin in a dose-dependent manner, while results for merlin full-length isoform 1 binding to F-actin was indeterminate (Figure 1). Merlin also binds to β/γ-F-actin in cosedimentation assays performed with the N-terminus. Although a significant increase in merlin N-terminus and isoform 2 pelleting is demonstrated in the presence of actin as compared to pelleting in the absence of actin (self-pelleting), isoform 1 pelleting in the presence and absence of actin is almost indistinguishable. Similarly, we were unable to demonstrate actin binding activity using the merlin isoform 1 C-terminal segment, spanning amino acids 340-595, in cosedimentation assays due to the comparable levels of pelleted protein in the absence of actin (data not shown).

The interaction of merlin isoform 2 to actin was quantified using data from F-actin cosedimentation assays. We show that as increasing concentrations of GST-merlin isoform 2 (0.05-3.0 μM) are added to a constant concentration of F-actin (4 μM), the proportion of merlin sedimenting with the F-actin pellet increased until it saturated at ~ 2 μM of total merlin added

(Figure 2). Merlin sedimenting in the presence and absence of actin was quantified, and the difference compared to total merlin added was regarded as specifically bound. Scatchard analyses of these data provided a K_d of 3.6 ± 1.7 μM for merlin isoform 2 to actin binding and a saturated stoichiometric molar ratio of 1:11.5 (merlin:actin).

Previous reports have suggested that the presence of N-terminal tags on fusion proteins hinders the ability of recombinant ERM proteins to bind actin [31, 32, 39]. Although our results indicate that full-length isoform 2 and the N-terminal 1-332 GST-fusion proteins bind F-actin efficiently, we examined whether the inability of merlin isoform 1 to bind F-actin in cosedimentation assays were related to the presence of the GST tag. GST-cleaved merlin isoform 1 also does not demonstrate F-actin binding by cosedimentation assays. Likewise, we did not observe a significant difference in merlin N-terminus and isoform 2 binding to actin in the absence of GST (data not shown). Multiple cosedimentation assays consistently showed that merlin in the presence or absence of GST behaved similarly.

Merlin isoform 1 binds actin less effectively than the free N-terminus

To further examine if merlin isoform 1 is capable of binding F-actin, a solid-phase protein-protein binding assay was employed as an alternative approach [31]. This method, which was used to demonstrate the existence of the middle ezrin F- and G-actin binding sites, alleviates the aggregation problem of merlin. Titrated amounts of GST-merlin fusion proteins were coated in 96-well microtiter plates and incubated with constant amounts of F- or G-actin. Bound proteins were eluted in SDS-PAGE sample buffer and analyzed by immunoblotting. The results show that merlin isoform 1 binds F-actin, although less effectively than the N-terminus (Figures 3A, B). Similarly, merlin isoform 2 bound F-actin more effectively compared to isoform 1 in this

assay (data not shown). The C-terminus of isoform 1 (aa 340-595) failed to bind F-actin, and the BSA coated surface showed no F-actin binding (Figure 3B).

Merlin does not bind G-actin

One advantage of the solid-phase binding assay is that it can be used to detect binding of monomeric actin. Although a distinct G-actin binding site has been identified in the ezrin middle region (aa 281-310) [31, 32], we were unable to detect G-actin binding to merlin (data not shown). Concurrent with solid-phase binding assays, GST pull-down assays were performed as an alternative approach to examine merlin's ability to bind G-actin in vitro [35]. In these studies, equal amounts of GST-merlin fusion proteins were immobilized on GSH-sepharose beads and incubated with G-actin at a concentration of 0.05 μM (below the critical concentration). Bound proteins were resolved by SDS-PAGE and detected by Western blotting. As shown in Figure 4, GST pull-down assays did not reveal G-actin binding to merlin, confirming the results of the solid-phase binding assay. As controls, the G-actin binding protein, Wiscott Aldrich Syndrome interacting protein (WIP), bound G-actin strongly, while GST-Cdc42 and GST did not.

Merlin slows actin filament disassembly

To assess the role of merlin in actin filament dynamics, actin polymerization and depolymerization assays were conducted multiple times. Pyrene-labeled G-actin was polymerized to 1.5 μM by the addition of KCl and $MgCl_2$ to 0.1 M and 2 mM, respectively, in the presence of increasing amounts of GST-merlin fusion protein isoform 2, N-terminal 1-332 or GST (0.03-1.5 μM). We did not detect any alteration in the rate of actin polymerization in the presence of merlin indicating that merlin does not nucleate actin assembly (data not shown).

Next, to determine the kinetics of actin disassembly, pyrene F-actin (10 μM) was diluted to 0.2 μM in the absence or presence of GST-merlin isoform 2, N-terminal 1-332 or GST (control) at concentrations ranging from 0.002-1.0 μM. F-actin alone, as expected, rapidly disassembled upon dilution. Addition of either merlin isoform 2 or the N-terminus consistently slowed the rate of actin depolymerization in a dose-dependent manner (Figure 5). This, and the binding data, suggest that merlin may be binding to the sides of the actin filaments thereby stabilizing their lengths. Fluorescent readings taken at extended time-points indicated merlin prevents the disassembly of filaments. This data is further supported by the cytoskeletal localization of merlin by immunoelectron microscopy (Figure 6). Immunogold staining shows that merlin resides on cortical actin filaments, particularly near their ends where filaments intersect one another. This distribution suggests that merlin is targeted to these cytoskeletal locations by both its actin binding and membrane protein binding properties.

DISCUSSION

Merlin, as a tumor suppressor protein, represents a distinct member of the ERM protein family. Merlin differs from the ERM family members in being expressed as two major isoforms having alternate C-termini. Similar to ERM proteins, both endogenous and exogenous merlin in cultured cells concentrate in cell surface structures, such as membrane ruffles, microvilli and filopodia, where actin filaments associate with plasma membranes [24, 27]. A high affinity F-actin binding site present in the last 34 amino acids of ERM proteins is not conserved in merlin isoforms [1]. This is consistent with the observation that the C-terminal half of either merlin isoform, when expressed in cell culture, is not associated with stress fibers [25]. Recent studies document two actin binding domains within the N-terminal and middle regions of the ERM

proteins, which bind to F-actin and F-and G-actin, respectively [30, 31]. Compared to ERM proteins, merlin binding to actin is not well characterized. Blot overlay experiments performed with ^{125}I-labelled F-actin and merlin isoform 1 revealed no detectable binding to F-actin [18]. Actin cosedimentation assays performed with *in vitro* transcribed and translated products of merlin isoforms revealed binding to F-actin via the N-terminus with no difference in the ability of both isoforms to bind F-actin [33]. The actin cytoskeleton mediates a variety of dynamic functions including maintaining cell shape and regulating cell polarity, motility and division. Changes in the actin cytoskeleton of transformed cells, the role of adherence in transformation and metastasis, and the ability of some transforming genes to affect primarily cytoskeletal proteins, emphasize the significance of the actin cytoskeleton in cancer [40]. Defining merlin's normal function as a cytoskeleton-membrane linker protein and its role in actin assembly may be critical for understanding the basis for NF2 and NF2-related tumors. Toward this goal, we undertook a detailed biochemical characterization of the merlin-actin interaction and demonstrate differences between the two major merlin isoforms as well as between merlin and the ERM proteins.

While sharing several properties with ERM proteins, merlin differs from these proteins in its mode of interaction with the actin cytoskeleton. Subcellular distribution of merlin using detergent extraction methods demonstrates that merlin is recovered exclusively in the insoluble/cytoskeletal-associated fraction of cells [29, our unpublished data], differing from ERM proteins which distribute similarly to both the soluble and insoluble fractions [23, 28]. Employing actin cosedimentation assays, we demonstrate that the free N-terminus of merlin and full-length merlin isoform 2 are capable of binding to actin through a N-terminal actin-binding region that was identified in ezrin [31]. Furthermore, we show that merlin isoform 2 to actin

binding is saturable with a dissociation constant of ~ 3.6 μM and a stoichiometric association of 12 actin molecules bound per merlin molecule. Other studies have shown that ezrin binds to actin in a saturable manner with a molar ratio of about 1:10 (ezrin:actin) and with dissociation constants which vary from ~50nM to 500nM [31, 41]. Another recent study elegantly demonstrates that phosphorylated moesin interacts with F-actin with a relatively high affinity (K_d~1.5 nM) and a maximum stoichiometry of 1:1 [23]. Thus, merlin appears to bind actin with a lower affinity than reported for ERM proteins. By cosedimentation assays, we were unable to observe merlin isoform 1 binding to actin, which is contrary to a previously published report [33]. However, we do show that merlin isoform 1 binds actin using the solid-phase binding assay, although to a lesser extent as compared to the free N-terminus. Unlike ezrin, which binds both F- and G-actin [31], merlin does not demonstrate G-actin binding under the same assay conditions.

Merlin's influence on the kinetics of actin disassembly differs from ezrin, which has been reported to promote pyrene-labeled actin assembly, with predominant effects on filament elongation of β-actin [41]. Merlin has no effect on actin polymerization, but is able to inhibit actin depolymerization in a dose-dependent manner. This observation indicates that the stabilizing effect is not due to capping of the ends of actin filaments, and suggests that merlin probably stabilizes F-actin through a lateral association. The latter possibility is further supported by electron microscopy data, which illustrate merlin residing along filament lengths, most highly concentrated at cortical actin-rich regions. Among the ERM proteins, radixin is shown to exhibit actin barbed-end binding activity, while moesin and ezrin appear to bind to the sides of the filaments [4, 22, 41-43].

PIP_2 binding and phosphorylation of a specific C-terminal threonine (Thr) residue of ERM proteins are known to generate and/or maintain the open conformation of the ERM proteins, allowing them to interact with their membrane partners [3, 4, 38]. However, phosphorylation of this Thr residue did not affect their ability to bind actin [38]. Interestingly, the regulation of the ERM-actin interaction has been established by a recent study which clearly demonstrates that in the presence of 0.1% Triton X-100, both PIP_2 and phosphorylation at Thr586 activates the high affinity F-actin binding site present at the C-terminus of platelet moesin [23]. We have observed that merlin isoform 1 binds F-actin less effectively than isoform 2, which could be explained by its interdomain self-association that masks the actin binding site in isoform 1. Our recent study documents that the *in vitro* interaction of merlin isoform 1 with its ligand NHE-RF is increased in the presence of PIP_2 [15]. However, our attempts to observe an increase in actin binding of recombinant merlin isoform 1 in the presence of Triton X-100 and PIP_2 was not successful by either cosedimentation or solid-phase binding assays (data not shown). It is possible that in addition to PIP_2, phosphorylation of a critical residue in merlin may be important for merlin isoform 1 to effectively bind actin. While, merlin is reported to be phosphorylated on serine/threonine residues [44, 45], the identity of the specific residues involved has not been defined. The critical Thr residue important for maintaining the active conformation of the ERM proteins is conserved in both isoforms of merlin, thus warranting further studies to determine if phosphorylation at this site is essential for the merlin isoform 1 interaction with the actin cytoskeleton.

Mutational analyses of both germline and somatic alterations in the *NF2* gene revealed a wide variety of inactivating mutations, the majority of which are predicted to truncate the protein. Interestingly, no mutations have been reported in either exon 16 or exon 17 implying

that both merlin isoforms may be necessary for tumor suppressor function [1]. Structure-function analyses performed with naturally occurring *NF2* mutations reveal a significant increase in detergent solubility of mutant merlin compared to wild type, indicating a decreased ability of mutant merlin to interact with the cytoskeleton. Localization studies further demonstrated that many of the mutants likely to impair tumor suppressor activity of merlin failed to maintain a stable interaction with actin [29, 46]. Merlin isoform 2 due to its 'open' state is able to interact more effectively with NHE-RF and the actin cytoskeleton than merlin isoform 1 where the equivalent sites are masked in the 'closed' state. NHE-RF links merlin isoforms to various ion channels and receptors that provide new possibilities for effects on intracellular signaling. Merlin isoform 2 in its constitutive active state is likely to have more effects on intracellular signaling mediated either through NHE-RF or other partners and thus may have a distinct role compared to merlin isoform 1.

The key players controlling actin cytoskeletal organization are the Rho-GTPase family members, Rho, Rac and Cdc42. They are believed to act as molecular switches regulating signal transduction pathways that link membrane receptors to the cytoskeleton [47, 48]. The N-terminal halves of the ERM proteins bind to the RhoGDP dissociation inhibitor (RhoGDI), releasing bound GDP-Rho from RhoGDI, and initiating the activation of Rho family members [49]. Rho-kinase, a downstream target of active Rho can phosphorylate ERM proteins *in vitro*, stabilizing the active state of these proteins [38]. Thus, ERM proteins are clearly implicated in the Rho-GTPase signaling pathway. Based on the N-terminal sequence similarity of merlin with the ERM family members, the ability of merlin's N-terminus to bind RhoGDI was tested and found to bind RhoGDI [28]. Merlin's role in the small Rho-GTPase signaling cascade is not yet defined. By acting as a linker connecting plasma membrane proteins to the actin cytoskeleton,

merlin is likely to be an active player in this signaling cascade leading to actin reorganization, the disruption of which may lead to NF2 related tumors.

ACKNOWLEDGMENTS

We thank Dr. K. Barkalow for advice on actin fluorescence measurements. We also thank Dr. N. Ramesh for generously providing purified N-WIP and for valuable discussions. The technical expertise of Denise Pinney-Michalowski is gratefully acknowledged. We thank members of our laboratory for helpful comments on the manuscript. This work was supported by NIH grant NS24279, U.S. Army grant (VR) and NIH HL56949 (JH). MFJ was supported by NRSA post-doctoral fellowship from NIH F32-NS10699.

REFERENCES

1 Gusella, J. F., Ramesh, V., MacCollin, M. and Jacoby, L. B. (1999) Biochim Biophys Acta **1423**, M29-36

2 Chishti, A. H., Kim, A. C., Marfatia, S. M., Lutchman, M., Hanspal, M., Jindal, H., Liu, S. C., Low, P. S., Rouleau, G. A., Mohandas, N., Chasis, J. A., Conboy, J. G., Gascard, P., Takakuwa, Y., Huang, S. C., Benz, E. J., Jr., Bretscher, A., Fehon, R. G., Gusella, J. F., Ramesh, V., Solomon, F., Marchesi, V. T., Tsukita, S., Hoover, K. B. and et al. (1998) Trends Biochem Sci **23**, 281-2

3 Bretscher, A. (1999) Curr. Opin. Cell. Biol. **11**, 109-116

4 Tsukita, S. and Yonemura, S. (1999) J Biol Chem **274**, 34507-10

5 Reczek, D., Berryman, M. and Bretcher, A. (1997) J. Cell. Biol **139**, 169-179

6 Murthy, A., Gonzalez-Agosti, C., Cordero, E., Pinney, D., Candia, C., Solomon, F., Gusella, J. and Ramesh, V. (1998) J. Biol. Chem. **273**, 1273-1276

7 Yun, C. H., Lamprecht, G., Foster, D. V. and Sidor, A. (1998) J. Biol. Chem. **273**, 25856-25863

8 Hall, R. A., Ostedgaard, L. S., Premont, R. T., Blitzer, J. T., Rahman, N., Welsh, M. J. and Lefkowitz, R. J. (1998) Proc Natl Acad Sci **95**, 8496-501

9 Hall, R. A., Premont, R. T., Chow, C. W., Blitzer, J. T., Pitcher, J. A., Claing, A., Stoffel, R. H., Barak, L. S., Shenolikar, S., Weinman, E. J., Grinstein, S. and Lefkowitz, R. J. (1998) Nature **392**, 626-30

10 Short, D. B., Trotter, K. W., Reczek, D., Kreda, S. M., Bretscher, A., Boucher, R. C., Stutts, M. J. and Milgram, S. L. (1998) J Biol Chem **273**, 19797-801

11 Wang, S., Raab, R. W., Schatz, P. J., Guggino, W. B. and Li, M. (1998) FEBS Lett **427**, 103-8

12 Bernardo, A. A., Kear, F. T., Santos, A. V., Ma, J., Steplock, D., Robey, R. B. and Weinman, E. J. (1999) J Clin Invest **104**, 195-201

13 Breton, S., Wiederhold, T., Marshansky, V., Nsumu, N. N., Ramesh, V. and Brown, D. (2000) J Biol Chem

14 Scoles, D. R., Huynh, D. P., Morcos, P. A., Coursell, E. R., Robinson, N. G. G., Tamanoi, F. and Pulst, S. M. (1998) Nat. Genet. **18**, 354-359

15 Gonzalez-Agosti, C., Wiederhold, T., Herndon, M. E., Gusella, J. and Ramesh, V. (1999) J Biol Chem **274**, 34438-34442

16 Sherman, L., Xu, H. M., Geist, R. T., Saporito-Irwin, S., Howells, N., Ponta, H., Herrlich, P. and Gutmann, D. H. (1997) Oncogene **15**, 2505-9

17 Gronholm, M., Sainio, M., Zhao, F., Heiska, L., Vaheri, A. and Carpen, O. (1999) J Cell Sci **112**, 895-904

18 Huang, L., Ichimaru, E., Pestonjamasp, K., Cui, X., Nakamura, H., Lo, G. Y. H., Lin, F. I. K., Luna, E. J. and Furthmayr, H. (1998) Biochm. Biophy. Res. Comm. **248**, 548-553

19 Hirao, M., Sato, N., Kondo, T., Yonemura, S., Monden, M., Sasaki, T., Takai, Y., Tsukita, S. and Tsukita, S. (1996) J Cell Biol **135**, 37-51

20 Turunen, O., Wahlström, T. and Vaheri, A. (1994) J. Cell Biol. **126**, 1445-1453

21 Martin, M., Andreoli, C., Sahuquet, A., Montcourrier, P., Algrain, M. and Mangeat, P. (1995) J. Cell Biol. **128**, 1081-1093

22 Pestonjamasp, K., Amieva, M. R., Strassel, C. P., Nauseef, W. M., Furthmayr, H. and Luna, E. J. (1995) Mol. Biol. Cell **6**, 247-259

23 Nakamura, F., Huang, L., Pestonjamasp, K., Luna, E. J. and Furthmayr, H. (1999) Mol Biol Cell **10**, 2669-85

24 Gonzalez-Agosti, C., Xu, L., Pinney, D., Beauchamp, R., Hobbs, W., Gusella, J. and Ramesh, V. (1996) Oncogene **13**, 1239-1247

25 Xu, L., Gonzalez-Agosti, C., Beauchamp, R., Pinney, D., Sterner, C. and Ramesh, V. (1998) Exp. Cell. Res, 231-240

26 den Bakker, M. A., Riegman, P. H., Hekman, R. A., Boersma, W., Janssen, P. J., van der Kwast, T. H. and Zwarthoff, E. C. (1995) Oncogene **10**, 757-63

27 Sainio, M., Zhao, F., Heiska, L., Turunen, O., den Bakker, M., Zwarthoff, E., Lutchman, M., Rouleau, G. A., Jaaskelainen, J., Vaheri, A. and Carpen, O. (1997) J Cell Sci **110**, 2249-60

28 Maeda, M., Matsui, T., Imamura, M. and Tsukita, S. (1999) Oncogene **18**, 4788-97

29 Deguen, B., Merel, P., Goutebroze, L., Giovannini, M., Reggio, H., Arpin, M. and Thomas, G. (1998) Hum Mol Genet **7**, 217-26

30 Martin, M., Roy, C., Montcourrier, P., Sahuquet, A. and Mangeat, P. (1997) Mol. Biol. Cell **8**, 1543-1557

31 Roy, C., Martin, M. and Mangeat, P. (1997) J. Biol. Chem. **272**, 20088-20095

32 Mangeat, P., Roy, C. and Martin, M. (1999) Trends Cell Biol **9**, 187-92

33 Xu, H. and Gutman, D. H. (1998) J. Neroscience Res **51**, 403-415

34 Hartwig, J. H. (1992) J Cell Biol **118**, 1421-42

35 Rohatgi, R., Ma, L., Miki, H., Lopez, M., Kirchhausen, T., Takenawa, T. and Kirschner, M. W. (1999) Cell **97**, 221-31

36 Barkalow, K., Witke, W., Kwiatkowski, D. J. and Hartwig, J. H. (1996) J Cell Biol **134**, 389-99

37 Hartwig, J. H. and DeSisto, M. (1991) J Cell Biol **112**, 407-25

38 Matsui, T., Maeda, M., Doi, Y., Yonemura, S., Amano, M., Kaibuchi, K., Tsukita, S. and Tsukita, S. (1998) J. Cell Biol. **140**, 647-657

39 Henry, M. D., Agosti, C. G. and Solomon, F. (1995) J. Cell Biol. **129**, 1007-1022

40 Hall, A. (1994) Ann. Rev. Cell. Biol. **10**, 31-54

41 Yao, X., Cheng, L. and Forte, J. G. (1996) J. Biol. Chem. **271**, 7224-7229

42 Tsukita, S., Hieda, Y. and Tsukita, S. (1989) J Cell Biol **108**, 2369-2382

43 Shuster, C. B. and Herman, I. M. (1995) J. Cell Biol. **128**, 837-848

44 Shaw, R. J., Henry, M., Solomon, F. and Jacks, T. (1998) Mol Biol Cell **9**, 403-19

45 Takeshima, H., Izawa, I., Lee, P. S., Safdar, N., Levin, V. A. and Saya, H. (1994) Oncogene **9**, 2135-44

46 Stokowski, R. P. and Cox, D. R. (2000) Am J Hum Genet **66**, 873-91

47 Hall, A. (1998) Science **280**, 2074-5

48 Bishop, A. L. and Hall, A. (2000) Biochem J **348 Pt 2**, 241-55

49 Takahashi, K., Sasaki, T., Mammoto, A., Takaishi, K., Kameyama, T., Tsukita, S., Tsukita, S. and Takai, Y. (1997) J. Biol. Chem. **272**, 23371-23375

ABBREVIATIONS

Abbreviations used: NF2, neurofibromatosis 2; NHE-RF, regulatory cofactor of Na^+-H^+ exchanger; PIP_2, phosphatidylinositol 4,5-bisphosphate; GST, glutathione *S*-transferase; aa, amino acid(s); GSH, glutathione; PAGE, polyacrylamide gel electrophoresis; MERM, merlin and ERM proteins; FERM, 4.1 and ERM proteins.

FIGURE LEGENDS

Figure 1 Actin cosedimentation with GST-merlin fusion constructs GST-merlin N-terminus 1-332, full-length isoform 1 (aa 1-595) or isoform 2 (aa 1-590), at concentrations ranging from 0.1-3.0 μM, were incubated with and without 4 μM F-actin and subjected to high-speed centrifugation at 200,000 ***g*** to pellet F-actin. Pelleted proteins were resuspended in SDS-PAGE sample buffer, separated on a 10% SDS-PAGE and transferred to nitrocellulose for immunoblot detection of merlin using the N21 antibody. GST control samples did not pellet in the absence or presence of F-actin (data not shown). The integrity of the F-actin in the pellet was visualized by Ponceau S staining of the nitrocellulose. Each assay is representative of three separate experiments for each merlin construct.

Figure 2 Saturation and Scatchard analyses of GST-merlin isoform 2 Variable concentrations of GST-merlin isoform 2 (0.05-3.0 μM) were incubated with a constant concentration of F-actin and assayed as described in Figure 2. Merlin cosedimenting with F-actin was quantified by Scanning Flour-S Analysis of immunoblots after subtracting values obtained from self-pelleting (- actin) and compared to total merlin added at each concentration. GST-merlin isoform 2 saturates actin at approximately 2 μM total merlin added. Linear transformation (Scatchard plot) provides a K_d of 3.6 ± 1.7 μM with ~12 actin molecules bound per molecule of merlin isoform 2. These data are the mean ± S.D. of three separate measurements.

Figure 3 Solid-phase protein-protein binding assay **(A)** The interaction of GST-cleaved merlin isoform 1 and F-actin were examined by coating titrated-merlin concentrations onto 96-well microtiter plates and overlaying with a constant concentration of F-actin (5 μM).

Unbound proteins were washed and merlin-to-actin-binding was determined after eluting bound proteins with SDS-PAGE sample buffer, separating by SDS-PAGE and Western blotting using merlin N21 and actin antibodies. **(B)** A constant concentration of GST-cleaved merlin isoform 1, N-terminus 1-332 and C-terminus 340-595 (2 μM) were coated on microtiter plates and examined for F-actin binding. BSA (2 μM) was coated as a control for non-specific F-actin binding. Reproducible results were obtained in five independent binding assays.

Figure 4 G-actin affinity pull-down assay GST-merlin fusion proteins were immobilized on GSH-sepharose beads and tested for their ability to pull down G-actin *in vitro*. The presence of G-actin binding to merlin-GSH sepharose was assayed by immunoblotting using an actin specific antibody. The N-terminus of WIP was used as a positive control for G-actin binding. Purified actin was added to the final lane as an actin antibody control. These assays were performed three times with similar results.

Figure 5 Merlin slows F-actin disassembly in pyrene-labeled assay Pyrene F-actin (10 μM), in the presence or absence of various concentrations of GST-merlin fusion proteins (0.004-0.2 μM), was diluted to 0.2 μM using monomer buffer and the decrease in fluorescence intensity was followed over time. Shown is a representative disassembly assay performed at least five times.

Figure 6 Localization of merlin in the cortex of a meningioma cell determined in the electron microscope Merlin was detected in the Triton X-100 insoluble cytoskeleton from a meningioma cell using the merlin-specific monoclonal antibody 1C4 followed by 10 nm

colloidal gold particles conjugated to goat anti-mouse IgG. Immunogold-labeled specimens were photographed after rapid-freezing, freeze-drying, and tantalum-tungsten and carbon-coating in a JEOL 1200-EX electron microscope. Gold particles of merlin on the cytoskeleton are highlighted in gold using Adobe PhotoShop software to add the color to the micrograph. Bar, 100 nm.

Figure 1.

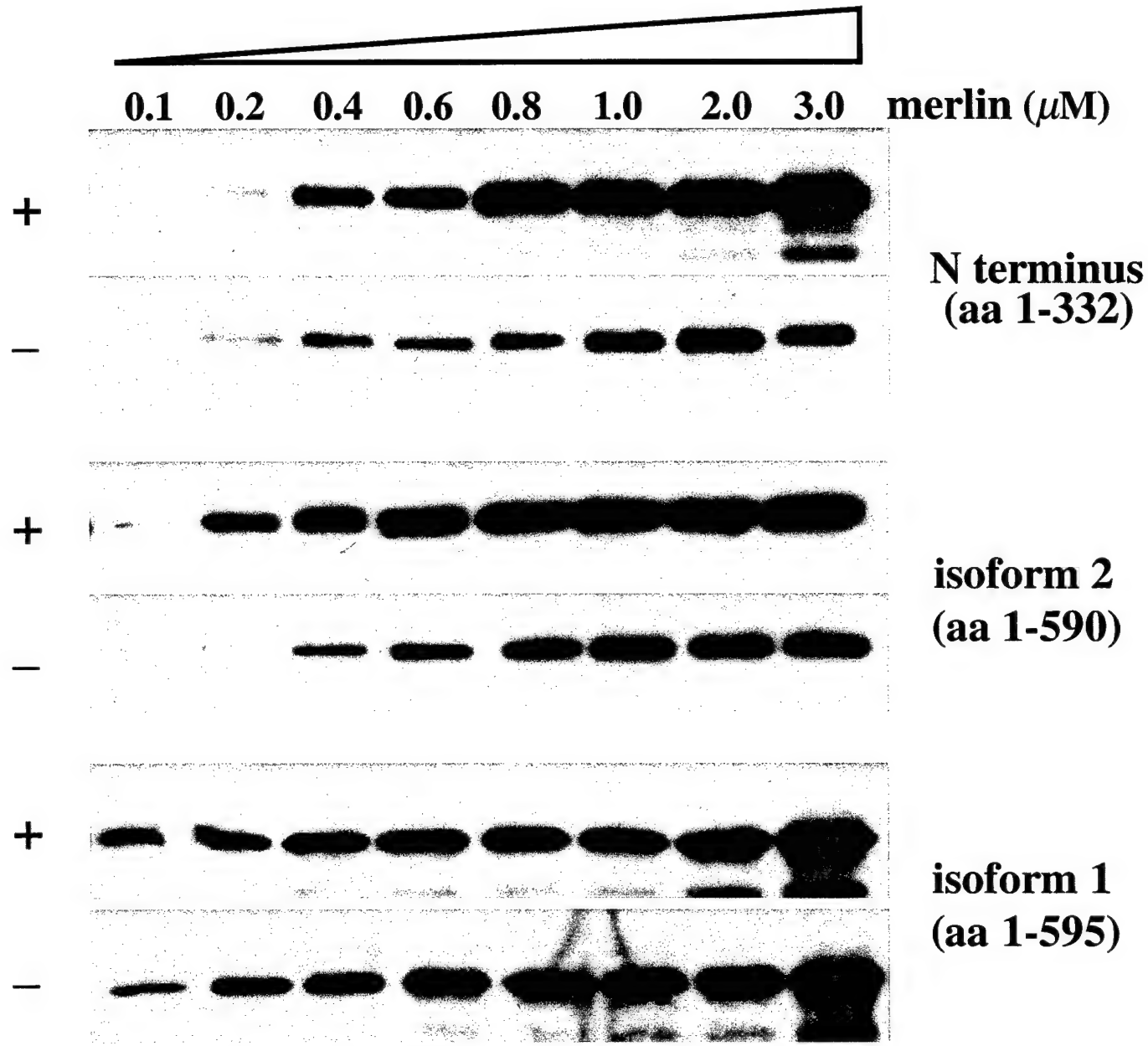
0.1
0.2
0.4
0.6
0.8
1.0
2.0
3.0
merlin (μM)
+
–
N terminus
(aa 1-332)
F-actin
(4μM)
+
–
isoform 2
(aa 1-590)
+
–
isoform 1
(aa 1-595)

Figure 2.

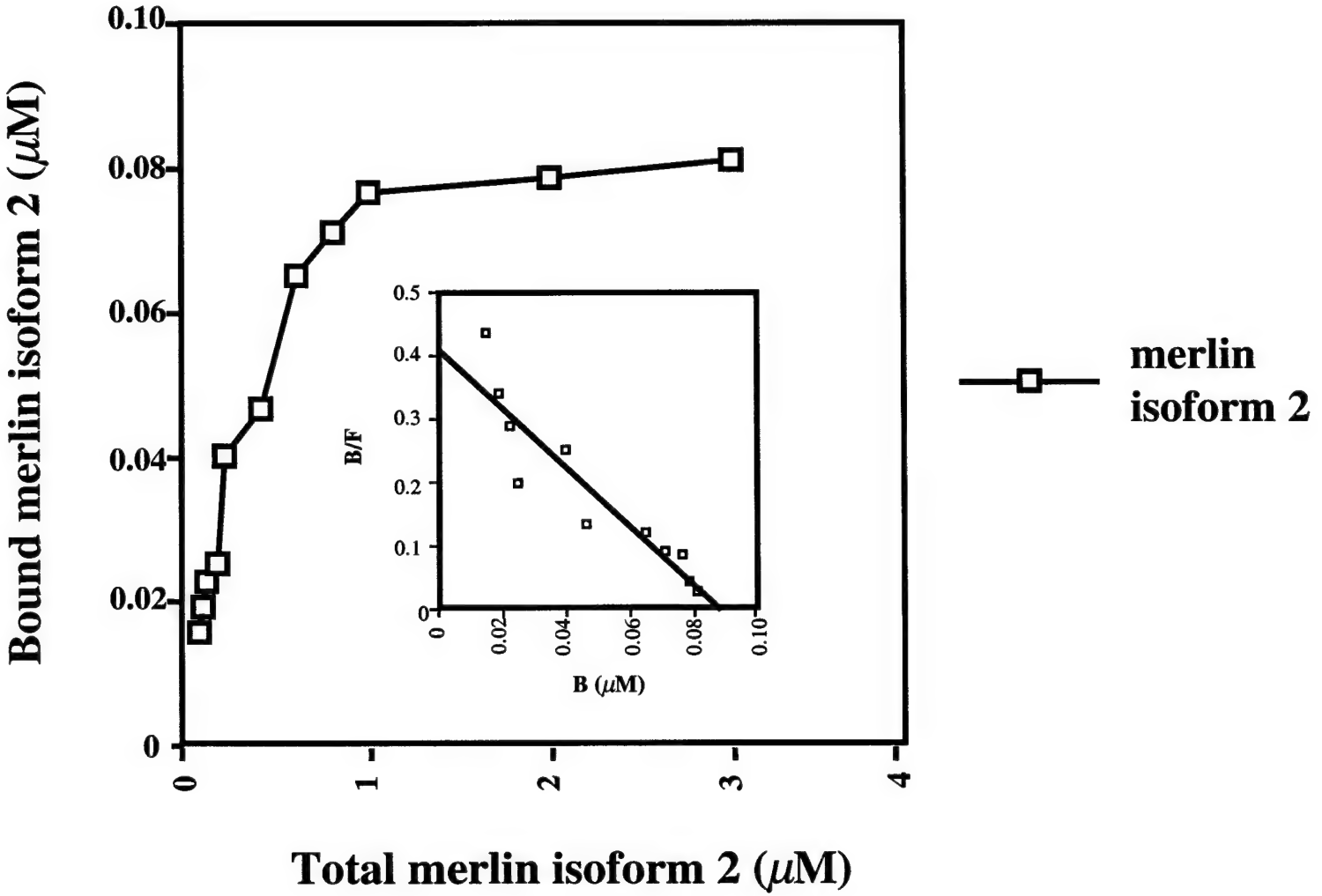
Bound merlin isoform 2 (μM)
0.10
0.08
0.06
0.04
0.02
0
0
1
2
3
4
Total merlin isoform 2 (μM)
B/F
0.5
0.4
0.3
0.2
0.1
0
0.02
0.04
0.06
0.08
0.10
B (μM)
merlin isoform 2

Figure 3.

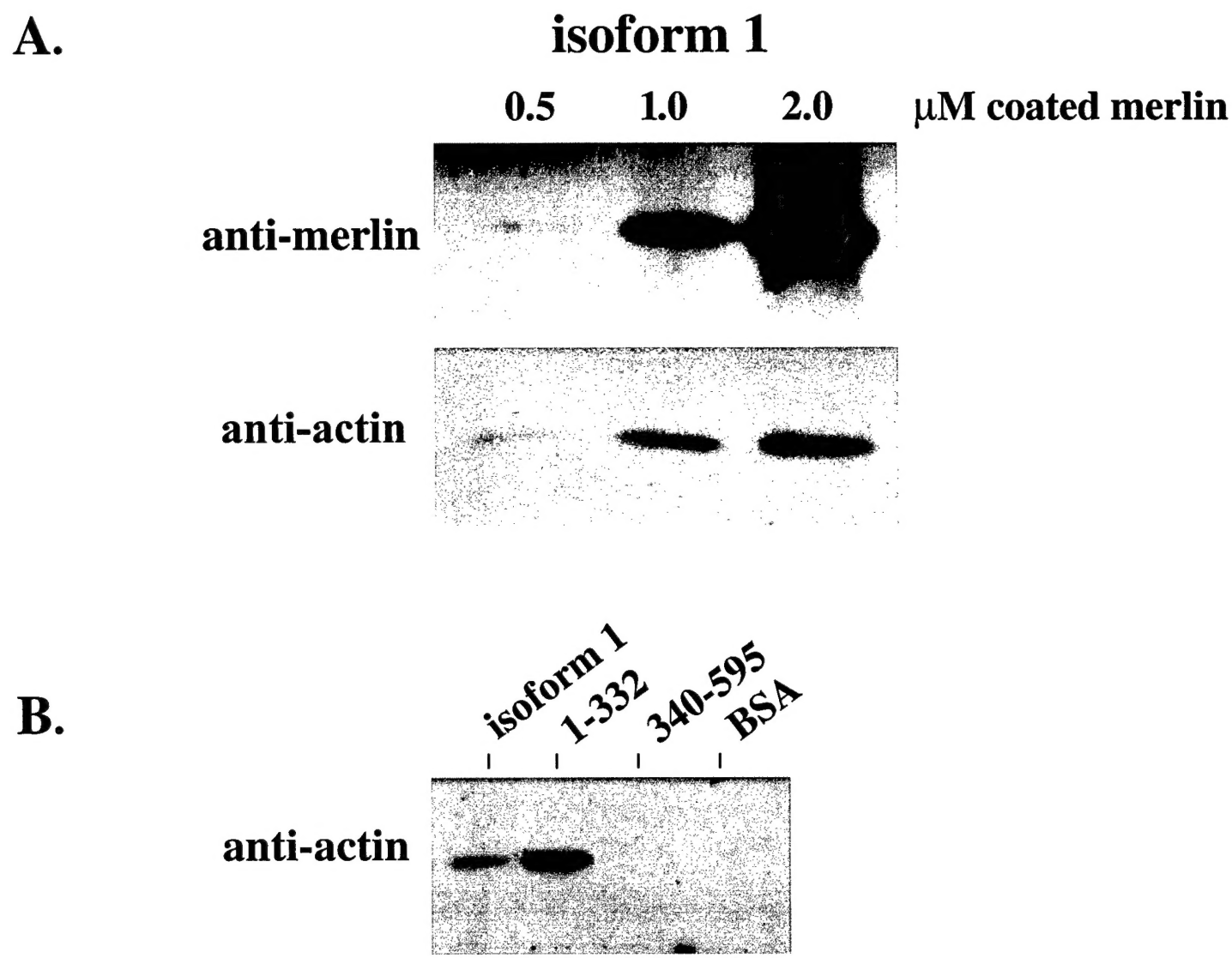
A.
isoform 1
0.5
1.0
2.0
μM coated merlin
anti-merlin
anti-actin
B.
isoform 1
1-332
340-595
BSA
anti-actin

Figure 4.

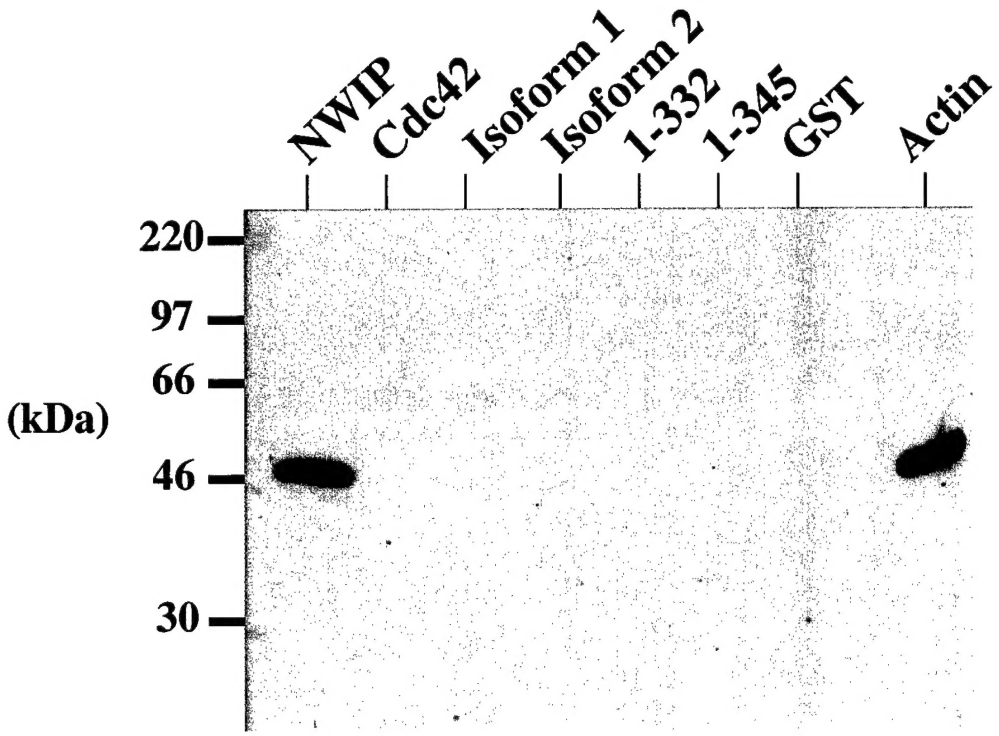
NWIP
Cdc42
Isoform 1
Isoform 2
1-332
1-345
GST
Actin
220
97
66
46
30
(kDa)

Figure 5.

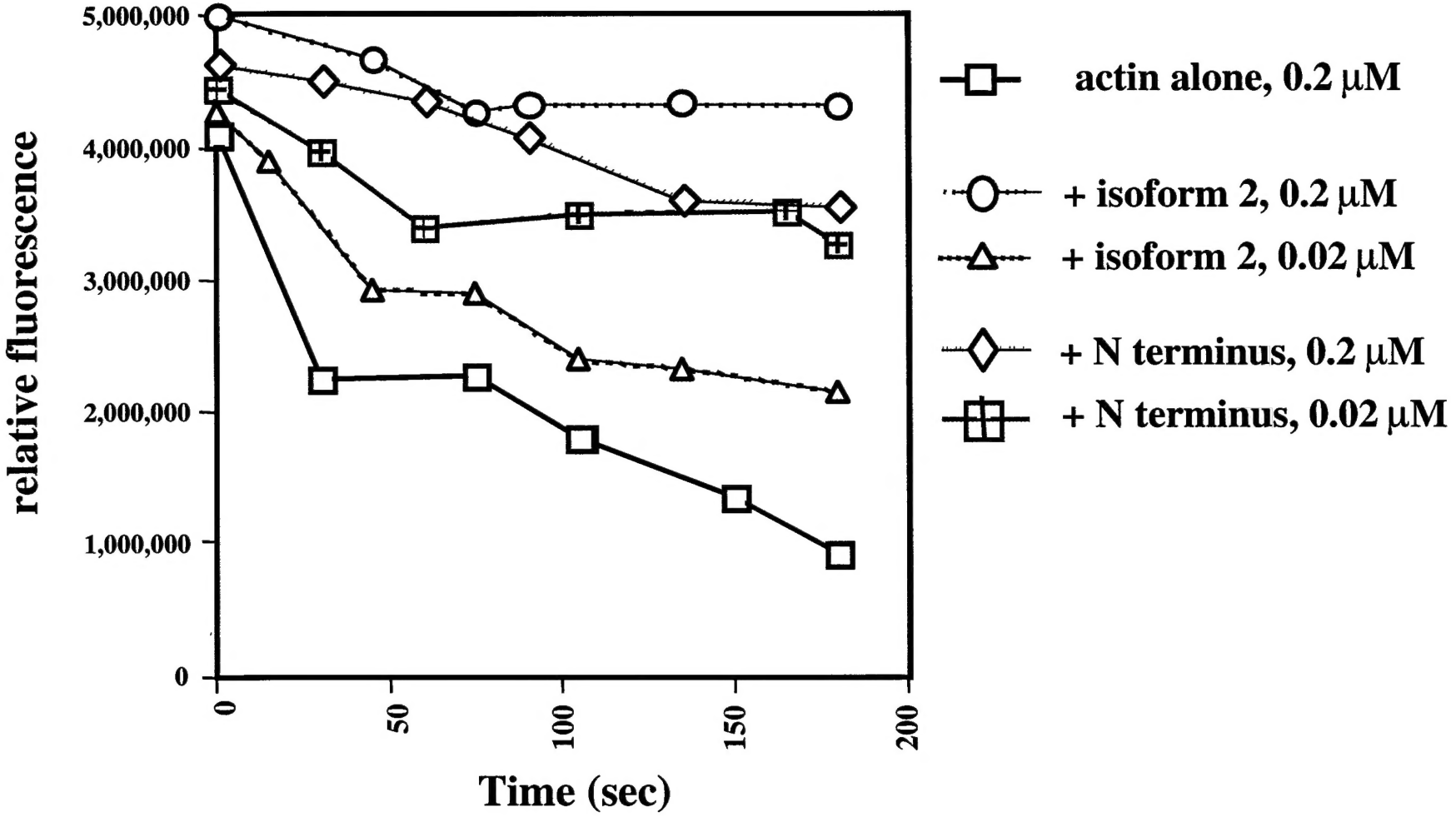
5,000,000
4,000,000
3,000,000
2,000,000
1,000,000
0
relative fluorescence
0
50
100
150
200
Time (sec)
actin alone, 0.2 μM
+ isoform 2, 0.2 μM
+ isoform 2, 0.02 μM
+ N terminus, 0.2 μM
+ N terminus, 0.02 μM

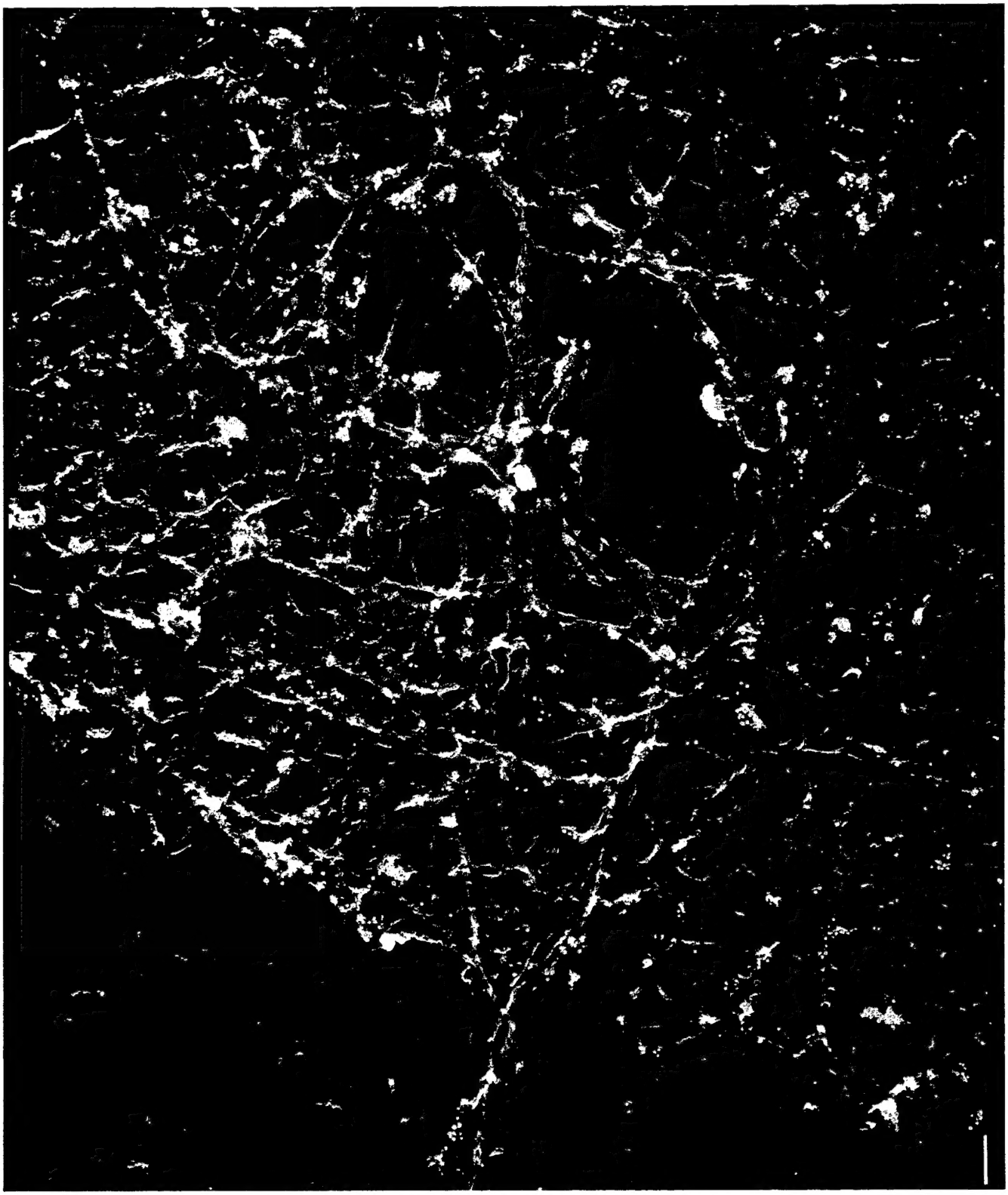

FIGURE 6